Episodic intrusion, internal differentiation, and hydrothermal alteration of the Miocene Tatoosh intrusive suite south of Mount Rainier, Washington

Edward A. du Bray[1,†], Charles R. Bacon[2], David A. John[3], Joseph L. Wooden[4,§], and Frank K. Mazdab[4,#]
[1]*U.S. Geological Survey-MS 973, Box 25046, Denver Federal Center, Lakewood, Colorado 80225, USA*
[2]*U.S. Geological Survey-MS 910, 345 Middlefield Road, Menlo Park, California 94025, USA*
[3]*U.S. Geological Survey-MS 901, 345 Middlefield Road, Menlo Park, California 94025, USA*
[4]*U.S. Geological Survey, Stanford–USGS Ion Microprobe Laboratory, Green Earth Sciences Research Building, Stanford, California 94305, USA*

ABSTRACT

The Miocene Tatoosh intrusive suite south of Mount Rainier is composed of three broadly granodioritic plutons that are manifestations of ancestral Cascades arc magmatism. Tatoosh intrusive suite plutons have individually diagnostic characteristics, including texture, mineralogy, and geochemistry, and apparently lack internal contacts. New ion-microprobe U-Pb zircon ages indicate crystallization of the Stevens pluton ca. 19.2 Ma, Reflection-Pyramid pluton ca. 18.5 Ma, and Nisqually pluton ca. 17.5 Ma. The Stevens pluton includes rare, statistically distinct ca. 20.1 Ma zircon antecrysts. Wide-ranging zircon rare earth element (REE), Hf, U, and Th concentrations suggest late crystallization from variably evolved residual liquids. Zircon Eu/Eu*–Hf covariation is distinct for each of the Reflection-Pyramid, Nisqually, and Stevens plutons. Although most Tatoosh intrusive suite rocks have been affected by weak hydrothermal alteration, and sparse mineralized veins cut some of these rocks, significant base or precious metal mineralization is absent.

At the time of shallow emplacement, each of these magma bodies was largely homogeneous in bulk composition and petrographic features, but, prior to final solidification, each of the Tatoosh intrusive suite plutons developed internal compositional variation. Geochemical and petrographic trends within each pluton are most consistent with differential loss of residual melt, possibly represented by late aplite dikes or erupted as rhyolite, from crystal-rich magma. Crystal-rich magma that formed each pluton evidently accumulated in reservoirs below the present level of exposure and then intruded to a shallow depth. Assembled by episodic intrusion, the Tatoosh intrusive suite may be representative of midsized composite plutonic complexes beneath arc volcanoes.

INTRODUCTION

The genesis, evolution, and solidification of shallow crustal magma bodies have once again become the focus of lively debate within the geologic community, in part because current U-Pb analytical uncertainties (several hundreds of thousands of years by secondary ion mass spectrometry [SIMS]; as little as tens of thousands of years by thermal ionization mass spectrometry [TIMS]) are now commensurate with pluton solidification time scales. Hypotheses proposed by Glazner et al. (2004) and Coleman et al. (2004) have sparked reconsideration and refinement of concepts that concern pluton emplacement, differentiation, and solidification. Tatoosh intrusive suite rocks south of Mount Rainier represent an accessible and relatively well exposed example of the uppermost parts of an arc-related magmatic system that resulted in an ~12-km-diameter complex that was active for ~3 m.y. The Miocene Tatoosh intrusive suite, Mount Rainier National Park, Washington (Fig. 1), as defined herein, consists of at least three discrete plutons that capture differentiation and solidification processes operative in shallow crustal magma reservoirs. Conclusions regarding the Tatoosh intrusive suite should be broadly applicable to similar systems.

Glazner et al. (2004) and Coleman et al. (2004) used U-Pb TIMS geochronologic data to suggest that individual plutons represent incrementally emplaced and solidified magma additions assembled over millions of years, a process that accordingly limits opportunities for either in situ homogenization or differentiation. In contrast, Sisson (2005), Zak and Paterson (2005), Hildreth and Wilson (2007), Lipman (2007), and Moore and Sisson (2008) contend that geologic relations favor continuous development of large, relatively homogeneous, pluton-scale magma reservoirs (magma reservoir and chamber usage herein follows that of Miller and Wark, 2008, their fig. 5) that subsequently undergo varying amounts of internal differentiation. An advantage in studying shallowly emplaced, moderate-sized plutons such as those of the Tatoosh intrusive suite is that they solidified relatively rapidly, thereby preserving textural and compositional relations between framework crystals and interstitial melt. Identification of the processes that prevail during intrusion solidification is essential to understanding magma reservoir dynamics as well as reservoir solidification time scales. Dominant processes must be consistent with "…the textural, mineralogical, and compositional uniformity, systematic internal zoning, and inconspicuous internal contacts that characterize so many plutons" (Sisson, 2005, p. 39).

In order to identify processes that contributed to the genesis and evolution of shallow magma reservoirs represented by the plutons of the Tatoosh intrusive suite, we evaluated critical geologic relations preserved therein. Data presented here confirm that subdivision of the intrusive rocks south of Mount Rainer

[†]E-mail: edubray@usgs.gov
[§]Current address: Department of Geological and Environmental Sciences, Stanford University, Stanford, California 94025, USA
[#]Current address: Department of Geosciences, 1040 E. 4th St., Gould-Simpson Building (Bldg. 77), University of Arizona, Tucson, Arizona 85721, USA

GSA Bulletin; March/April 2011; v. 123; no. 3/4; p. 534–561; doi: 10.1130/B30095.1; 11 figures; 7 tables; Data Repository item 2011018.

into three plutons (Wright, 1961) is justified by geographic distributions of rock masses (plutons) that have distinct and internally consistent texture, fabric, and geochemical characteristics. Whole-rock compositions were used to further characterize evolution of the Tatoosh intrusive suite. In places, especially on Mazama Ridge, rocks of the Tatoosh intrusive suite are weakly mineralized and preserve the transition from magmatic to hydrothermal processes. Zircon U-Pb ages were determined in order to establish the number, periodicity, and duration of magmatic events represented by the Tatoosh intrusive suite. The new age results indicate that the Tatoosh intrusive suite south of Mount Rainier was emplaced in three or more pulses at ca. 19.2, 18.5, and 17.5 Ma, and each pulse of magma was solidified before the next intruded. Zircon antecrysts (crystals formed in their host magma system, as broadly defined, but not as phenocrysts in the liquid represented by solidified material in which they are entrained; Charlier et al., 2005) in the Stevens pluton indicate crystallization at ca. 20.1 Ma and recycling into the host magma. Rock compositions and textures are consistent with partial to nearly complete separation of interstitial melt from early formed crystals, followed by rapid crystallization of variably granopyhric groundmass. The composite intrusive suite appears to reflect periodic ascent of crystal-bearing magma from deeper sources.

GEOLOGIC SETTING

The Quaternary Cascades volcanic arc was preceded by almost 40 m.y. of essentially cospatial magmatism represented by igneous rocks preserved in the ancestral Cascades arc. These Tertiary volcanic rocks depict the onset of subduction and arc magmatism between central Washington and northern California (McBirney, 1978; White and McBirney, 1978; Priest, 1990). The continental magmatic arc environment produced a series of coalescing and mutually overlapping volcanic centers (Smith, 1993); their solidified, subjacent magma reservoirs are exposed locally as small intrusive centers that have been shallowly exhumed along the length

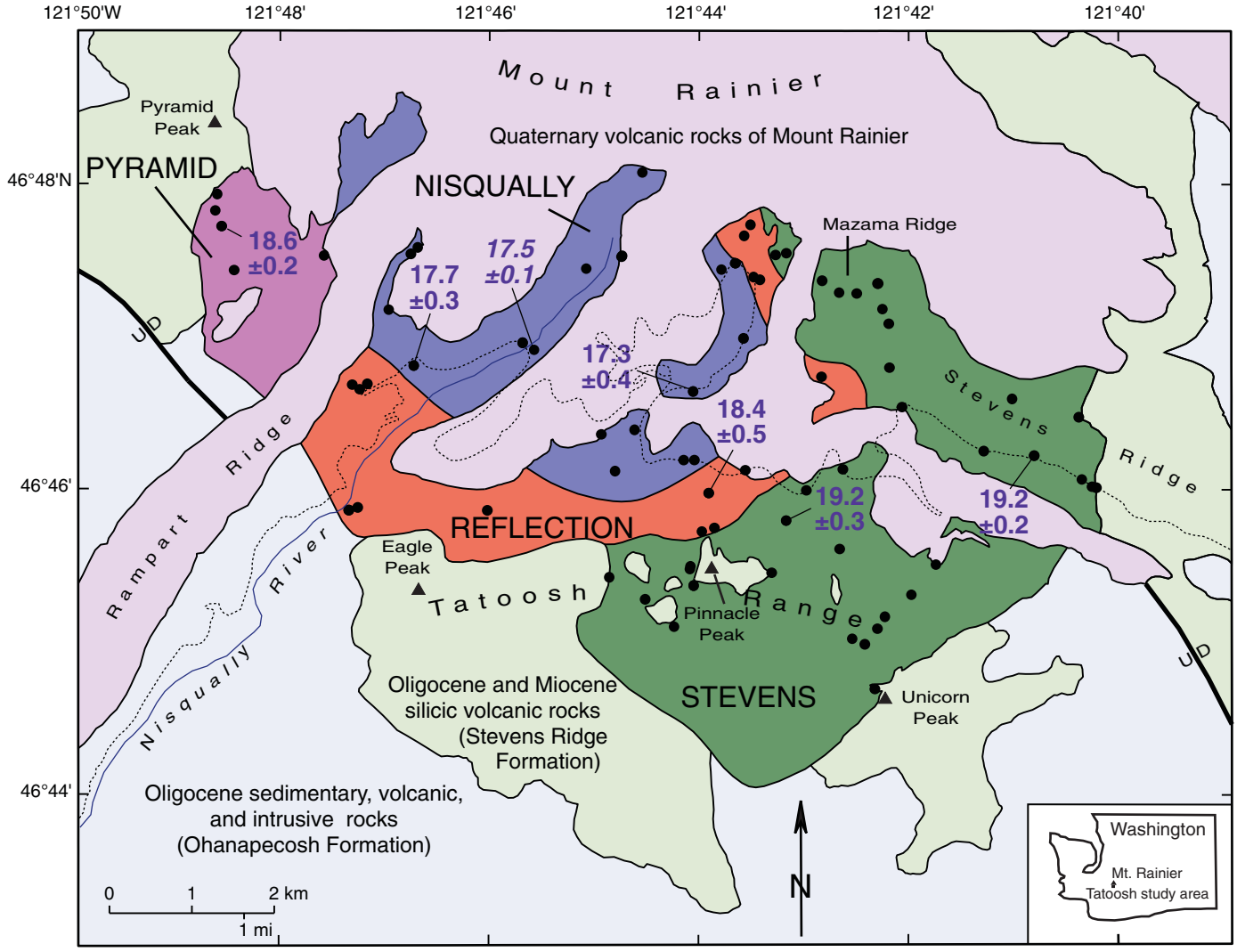

Figure 1. Generalized geologic map of the Tatoosh intrusive suite, Mount Rainier National Park, Washington (modified from Wright, 1961; Thompson, 1983). Pluton names are capitalized. Black dots identify geochemical sample sites. Numbers next to dots are new ion microprobe U-Pb zircon ages (in Ma); italicized *17.5 ± 0.1* indicates the sample location and age (in Ma) for a sample of the Nisqually pluton analyzed by Mattinson (1977). Dashed lines—main roads. Contacts—thin black lines. Faults—heavy black lines; U (up) and D (down) indicate relative sense of displacement across faults.

of the Cascade Range. These Tertiary intrusions, including those arrayed around the flanks of Mount Rainier, represent the unerupted parts of magma reservoirs that served as sources for eruptions from mafic shield volcanoes, intermediate composition stratovolcanoes, and intermediate through felsic volcanoes associated with caldera formation. In the area around Mount Rainier, the onset of ancestral arc magmatism is represented by the Oligocene Ohanapecosh Formation, which consists of as much as 3000 m of subaqueous and subaerial volcaniclastic and pyroclastic deposits and locally thick accumulations of basaltic andesite lava (Fiske et al., 1963). The Ohanapecosh Formation is overlain unconformably by the Oligocene-Miocene Stevens Ridge Formation of Fiske et al. (1963), which consists of 150 to ~900 m of subaerially deposited rhyodacite ash-flow tuff and associated volcaniclastic deposits. Zircon fission-track ages of ca. 27 Ma for two tuff samples from the Stevens Ridge Formation, and a U-Pb zircon TIMS age of 24.8 ± 0.3 Ma by J.M. Mattinson, were reported by Vance et al. (1987). The Stevens Ridge Formation is overlain by at least 700 m of Miocene Fifes Peak Formation, which is dominated by basalt, basaltic andesite, and andesite lava and associated volcaniclastic and pyroclastic deposits. Blakely et al. (2007) report $^{40}Ar/^{39}Ar$ ages of between 20.6 and 21.1 Ma for rocks of the Fifes Peak Formation just northwest of Mount Rainier. Elsewhere in the region, rocks mapped as Fifes Peak Formation include silicic ash-flow tuffs low in the unit. U-Pb zircon TIMS ages of 25.5 ± 0.1 Ma and 22.2 +0.3/–0.5 Ma by J.M. Mattinson, and likely inaccurate fission-track ages of ca. 7–20 Ma, prompted Vance et al. (1987) to suggest that the Stevens Ridge unit be considered a member of the Fifes Peak Formation. The youngest of these volcanic rocks are only slightly older than the Tatoosh intrusive suite, but they are nevertheless unrelated to those rocks.

Tertiary intrusive rock in the Mount Rainier environs was first noted more than a century ago. Subsequently, these rocks, including those in the Tatoosh Range on the south flank of the modern stratovolcano, were defined by Fiske et al. (1963) as the Tatoosh pluton. Pioneering work by Wright (1961), including subdivision of the intrusive rocks exposed south of Mount Rainier into discrete plutons, and subsequent conceptual refinements by Thompson (1983) provided a framework for our study.

Plutonic rocks in the Mount Rainier area are largely concealed by gently dipping to flat-lying (Wright, 1961; Fiske et al., 1963) roof remnants of the Ohanapecosh and Stevens Ridge Formations (including horizontally bedded rocks at and near Pinnacle Peak, Fig. 1), Quaternary surficial deposits (particularly glacial deposits), and volcanic rocks associated with Quaternary Mount Rainier. Consequently, contacts between Tatoosh intrusive suite plutons, although locally exposed in upper Paradise Valley, are rare, causing relative ages among most Tatoosh intrusive suite plutons to be indeterminate. Fiske et al. (1963, cross section G-G′) indicated that Tatoosh intrusive suite rocks were emplaced through nearly the full thickness of the Stevens Ridge Formation in the Tatoosh Range. Assuming that this area was also overlain by a full thickness of Fifes Peak Formation, the top of the Tatoosh intrusive suite probably was emplaced at a depth of at least 700 to ~1600 m, i.e., the nearby thickness of the Fifes Peak Formation. Fiske et al. (1963) described miaroles and vesicles, brecciated intrusive rock, and masses of very fine-grained to quenched rock atop the plutons of the Tatoosh intrusive suite consistent with their very shallow emplacement.

Fiske et al. (1963) argued for initiation of Tatoosh pluton emplacement by intrusion of numerous sills and subordinate dikes into host rocks composed of Ohanapecosh Formation and overlying Stevens Ridge Formation, followed by more voluminous intrusion of the main discordant plutons that crop out on the flanks of Mount Rainier. However, Mattinson (1977) determined U-Pb zircon ages of 26 Ma for a dioritic sill, part of a voluminous set of concordant intrusions in this area, ~22 km east of Mount Rainier's summit, and 14 Ma for a granodiorite pluton along the White River ~15 km, north-northeast of Mount Rainier. The 12 m.y. age difference between these rocks indicates that they are not plausibly part of a single magmatic episode. Similarly, field relations indicate that the plutonic masses intrude and truncate components of the sill and dike complex. Consequently, the notion that all of these intrusive bodies constitute the products of a single magmatic event is inconsistent with their designation as and inclusion in the Tatoosh pluton of Fiske et al. (1963); accordingly, we recommend abandonment of the Tatoosh pluton nomenclature.

As summarized by Bateman (1992, p. 26), intrusive rocks that "…crop out in the same general area and that have similar ages and similar or related compositions and fabrics may be combined into units of higher rank called intrusive suites." The group of three nested plutons exposed south of Mount Rainer fits these criteria and are therefore designated as the Tatoosh intrusive suite. Its constituent intrusive masses are (1) the Stevens pluton (named here for type exposures along the road through Stevens Canyon), (2) the Nisqually pluton (named here for type exposures south of the Nisqually Glacier), and (3) the Reflection-Pyramid pluton. Hereafter, the predominant mass of the Reflection-Pyramid pluton is referred to as the "Reflection phase" (named here for type exposures south of Reflection Lake), whereas its volumetrically minor, though distinctive, cumulate border component is referred to as the "Pyramid phase" (exposed on the ridge south of Pyramid Peak); "Reflection-Pyramid pluton" refers to the entire intrusive mass. These three plutons exclude other intrusive rocks formerly included within the Tatoosh pluton designation, including the sill and dike complex, the large composite (Mattinson, 1977) mass of intrusive rock exposed along the White River (14.1 Ma) and Sunrise Ridge (24.1 Ma) northeast of Mount Rainier, the Carbon River stock, and smaller intrusive rock outcrops arrayed on flanks of Mount Rainier. (See Fiske et al. [1963] for the distribution of Tertiary intrusive masses in the Mount Rainer vicinity.) A few new data for plutons at Sunrise Ridge and in the basins drained by the White and Carbon Rivers, although included in the GSA Data Repository (Tables DR1 and DR2)[1], are not further addressed. The Tatoosh intrusive suite is intruded by a variety of dikes that are compositionally similar to its constituent plutons. Excluding Quaternary rocks associated with development of the Mount Rainier stratocone, rocks of the Tatoosh intrusive suite are the youngest exposed in this area, which suggests that the dikes are not manifestations of younger, unrelated, presently undocumented volcanism. Similarly, geologic relations indicate that these dikes are not associated with the modern Mount Rainier magmatic system.

METHODS

Representative samples were collected across the discontinuously exposed Tatoosh intrusive suite plutons (Fig. 1). Whole-rock chemical analyses (85 samples), relative abundances of minerals (76 samples), plagioclase composition (4 samples), whole-rock isotopic data (4 samples), and zircon U-Pb geochronologic and trace-element data (6 samples) were acquired using methods fully described in the accompanying GSA Data Repository file (Item DR1 [see footnote 1]).

PETROGRAPHY OF TATOOSH INTRUSIVE SUITE ROCKS

Petrographic features of the three plutons included in the Tatoosh intrusive suite (Table 1) are individually distinctive and form coherent

[1]GSA Data Repository item 2011018, numerous additional data plots, tabular data, and ancillary text in support of this paper, which are explicitly cited in the text, is available at http://www.geosociety.org/pubs/ft2011.htm or by request to editing@geosociety.org.

TABLE 1. SUMMARY OF PETROGRAPHIC CHARACTERISTICS FOR TATOOSH INTRUSIVE SUITE CONSTITUENTS, MOUNT RAINIER NATIONAL PARK, WASHINGTON

Pluton/Phase	Nisqually	Pyramid	Reflection	Stevens
Averages, for *N* =	16	4	13	25
Quartz	19.7	5.7	16.6	19.3
Alkali feldspar	12.7	8.4	21.0	24.2
Plagioclase	52.4	59.4	48.6	47.4
Biotite	6.8	2.3	5.2	3.4
Hornblende	6.1	21.3	5.8	4.6
Pyroxene	1.3	3.0	2.6	0.4
Cpx/opx	C/o	O/c	C/o	C
Opaques	1.1	1.3	1.1	1.1
Color index	15.3	27.9	14.6	9.6
Median plagioclase composition, and content (range)				
Core	43 (36–53)	52 (51–56)	48 (26–57)	37 (29–43)
Interior	47 (35–64)	55 (34–58)	28 (24–30)	39 (37–41)
Rim	22 (21–30)	16 (8–25)	21 (18–23)	20 (16–24)
Opaque mineral characteristics				
Mt:Ilm	2:1	all Ilm	1:1	2:1
Mt exsolution	Hm	–	Ilm, Hm	Hm, Ilm
Ilm exsolution	Hm	Weak Hm	Hm, cores	Hm
Average grain size (microscopic visual estimate, mm)				
Quartz	1.1	0.5	0.7	0.6
Plagioclase	2.5	2.8	3.2	1.7
Alkali feldspar	1.0	0.4	1.0	0.7
Biotite	0.7	0.4	0.6	0.5
Hornblende	1.1	1.9	0.9	0.7
Pyroxene	1.0	0.7	1.4	0.5
Opaques	0.2	0.3	0.2	0.2
Morphology				
Quartz	a	a	a	a
Plagioclase	e–s	e	e	e–s
Alkali feldspar	a	a	a	a
Biotite	a–s	a	a–s	a
Hornblende	s–a	s	a	a–s
Pyroxene	–	e–s	s	a
Opaques	a	a	a	a
Grain size	medium	medium	medium	medium–fine

Note: Relative mineral abundances are average modal compositions, in volume percent (see GSA Data Repository file, Table DR3 [see text footnote 1]). Plagioclase compositions are for a subset of the geochronologically analyzed samples, determined by electron microprobe analysis. Cpx/opx indicates whether clinopyroxene (c), orthopyroxene (o), or both, are present; capital letter indicates dominant species. Morphology: a—anhedral; s—subhedral; e—euhedral. Opaque minerals: Mt—magnetite; Ilm—ilmenite; Hm—hematite.

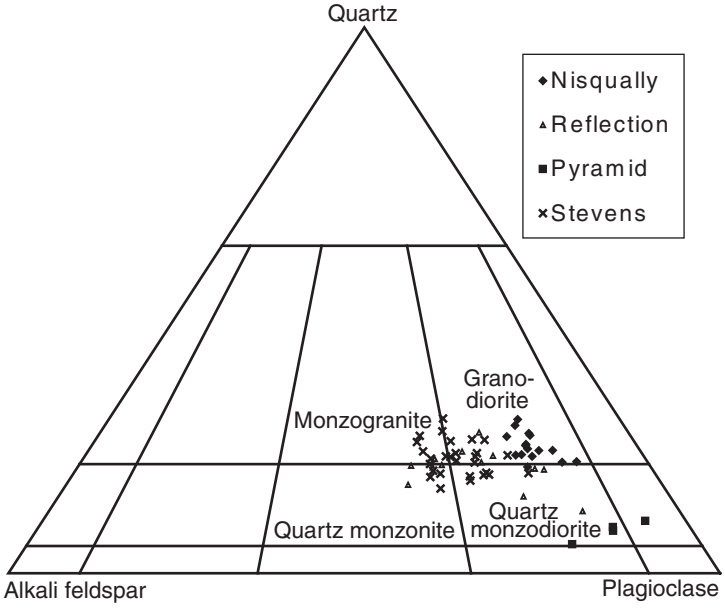

Figure 2. Quartz–alkali feldspar–plagioclase ternary diagram showing modal compositions of Tatoosh intrusive suite samples. Classification grid and rock names are those of Streckeisen (1976).

geospatial sample groupings (Fig. 1) consistent with discrete intrusive masses (Table DR3 [see footnote 1]). Following Streckeisen (1976), averages (and ranges) of ternary quartz, plagioclase, and alkali feldspar abundances (QAP) in Tatoosh intrusive suite rocks equate to the following rock names (Fig. 2): Stevens, granodiorite (monzogranite, quartz monzonite, and quartz monzodiorite); Nisqually, granodiorite (quartz monzodiorite); Reflection, granodiorite, excluding one unusually plagioclase-rich sample (monzogranite, granodiorite, quartz monzonite, and quartz monzodiorite); and Pyramid, quartz monzodiorite (quartz diorite). Modal data for the Nisqually and Stevens plutons and the Pyramid phase define coherent, mutually nonoverlapping QAP composition fields, whereas the composition of the Reflection phase varies significantly and overlaps the Stevens and, to a lesser extent, Nisqually pluton compositions. Samples of the Nisqually and Stevens plutons and the Reflection phase each contain distinctly more quartz (~20%) and have lower plagioclase–alkali feldspar ratios than the Pyramid phase. Plagioclase–alkali feldspar ratios also distinguish the Nisqually (higher) and Stevens (lower) plutons. A single sample (93T011), spatially associated with the Nisqually pluton, has petrographic features, particularly grain size, that are distinct relative to those of all other Nisqually samples. This sample is from an isolated outcrop on the south slope of Mount Rainier, and its features are sufficiently distinct to warrant possible identification of a separate intrusive mass, albeit sparingly exposed.

Intrusive rocks of the Tatoosh intrusive suite are medium grained (although the Stevens pluton is fine grained in some places) and hypidiomorphic inequigranular. Euhedral plagioclase laths (average 2–3 mm), hornblende (average 1 mm), and minor pyroxene (average 1 mm) are set in a fine-grained groundmass. Alkali feldspar is variably perthitic and cloudy, reflecting abundant fluid inclusions and incipient alteration to clay minerals and sericite, in all but the Nisqually pluton. Most plagioclase is moderately oscillatory zoned and albite twinned. Distinctive plagioclase in the Reflection phase is the most diagnostic feature of this intrusive body. These plagioclase laths are as much as 1 mm longer than in other plutons of the Tatoosh intrusive suite and are distinctively medium to dark gray as a consequence of abundant extremely fine-grained opaque oxide grains and needles concentrated in some plagioclase compositional zones. Samples of the Nisqually pluton and Reflection phase both contain ~15% total mafic minerals, whereas samples of the Stevens and Pyramid phase contain ~10% and 28%, respectively. Elevated mafic mineral contents characteristic of the Pyramid phase are in accord with

its bulk composition and cumulate texture, as indicated by elevated plagioclase and low quartz contents. Biotite and hornblende are ubiquitous constituents of all Tatoosh intrusive suite plutons. Abundances of pale-green to olive-green hornblende and straw yellow to red-brown biotite in samples of the Nisqually and Stevens plutons and in the Reflection phase are subequal, whereas hornblende is much more abundant than biotite in the Pyramid phase. Colorless to pale-tan or pale-green clinopyroxene is present in samples of all Tatoosh intrusive suite plutons (although rare in the Stevens pluton) that contain less than ~68% SiO_2, whereas colorless to rosy brown orthopyroxene is sporadically present in samples of all Tatoosh intrusive suite plutons (excluding the Stevens pluton) that contain less than ~66% SiO_2. Some pyroxene in the Reflection phase is replaced by secondary biotite and hornblende. Apatite (cloudy and brownish due to abundant tiny inclusions) and zircon are ubiquitous accessory minerals in Tatoosh intrusive suite plutons, whereas primary titanite and (or) allanite are present in a few samples.

Fine-grained (0.5–1 mm) groundmass (mesostasis) composed of interstitial quartz, alkali feldspar, and minor biotite is likely crystallized intergranular melt, a petrologically important component of all Tatoosh intrusive suite rocks. Granophyric intergrowths characterize the groundmass in all Tatoosh intrusive suite plutons, but they are almost ubiquitous in samples of the Stevens pluton. Most importantly, groundmass percentages vary significantly within each of the Tatoosh intrusive suite plutons (Fig. 3). Given crystal size systematics among the three plutons, these relations most plausibly indicate differential melt extraction and attendant crystal accumulation. The Stevens pluton contains the greatest groundmass abundances, whereas Pyramid samples are largely plagioclase-hornblende cumulates that contain minor trapped melt and therefore do not represent liquid compositions. Extracted melts are likely preserved as aplite dikes hosted by Tatoosh intrusive suite plutons.

The Stevens and Nisqually plutons and the Reflection phase contain coexisting titanomagnetite and ilmenite, whereas ilmenite is the only Fe-Ti oxide in the Pyramid phase; the Fe-Ti oxides display variable subsolidus exsolution effects (Item DR2 [see footnote 1]). Relative abundances of titanomagnetite and ilmenite vary from ~3:1 to 1:2 but average ~2:1 (Table 1). Some Stevens samples contain intergrown ilmenite and titanite; others contain sparse, small (≤5 μm) pyrrhotite or pyrite blebs within plagioclase and titanomagnetite. Magnetite and lesser ilmenite are intergrown with fine-grained, shreddy (hydrothermal) biotite in some Stevens pluton samples. The Pyramid phase contains coarser (to 35 μm), more abundant pyrrhotite blebs in ilmenite crystals. Titanomagnetite and ilmenite are included in plagioclase, pyroxene, hornblende, and (or) biotite; they are also concentrated in clots of mafic minerals in all but the Pyramid phase. Ilmenite is abundant as inclusions in plagioclase, biotite, and clinopyroxene and as disseminated crystals in the groundmass of the Pyramid phase. These intergrowth relations suggest relatively early Fe-Ti oxide crystallization.

The Stevens pluton includes a volumetrically minor but petrologically significant enclave-rich mafic variant exposed at pluton–roof rock contacts (along the northeast part of Mazama Ridge, near the Mazama Ridge breccia pipe [Wright, 1961], and at Pinnacle Peak) and along some pluton–wall-rock contact segments (east edge of pluton in Stevens Canyon). Diagnostic characteristics of this variant include fine grain size and uncharacteristically abundant mafic minerals (~20%). Together, these features suggest that these rocks represent relatively undifferentiated magma rapidly solidified along relatively cool host rock contacts. These hypidiomorphic inequigranular rocks contain euhedral laths of plagioclase (0.5–1 mm) and anhedral hornblende (0.5 mm) in a groundmass (weakly granophyric in some places) composed of anhedral 0.2 mm quartz, alkali feldspar, and Fe-Ti oxide minerals. Apatite and zircon are ubiquitous accessory minerals; secondary titanite is present as well.

Andesite to basaltic andesite and aplite dikes, between several centimeters and as much as a meter thick, are moderately abundant within the Tatoosh intrusive suite plutons. Phenocrysts (1–2 mm) of plagioclase, in an intersertal groundmass (0.05–0.2 mm) composed of plagioclase, Fe-Ti oxides, and hornblende, are a nearly ubiquitous feature of the fine-grained mafic dikes. Up to several percent clinopyroxene and (or) hornblende phenocrysts are also present in some mafic dikes. Apatite is the principal accessory mineral. Combinations of secondary titanite, biotite, epidote, chlorite, and (or) actinolite-tremolite indicate that many mafic Tatoosh intrusive suite dikes were affected by late-magmatic deuteric processes. Aplite dikes are principally composed of fine-grained xenomorphic inequigranular intergrowths of quartz, weakly perthitic alkali feldspar, and albite. Combinations of Fe-Ti oxides, red-brown biotite, and pale-green hornblende are minor constituents of the aplite dikes. Accessory minerals in the aplite dikes include apatite, zircon, and allanite. Granophyric to graphic intergrowths of quartz and alkali feldspar are especially common in Tatoosh intrusive suite aplite dikes.

Dark-colored mafic enclaves are present in all Tatoosh intrusive suite plutons, but they are most abundant in the Stevens pluton. Tatoosh intrusive suite enclaves are spherical to discoid in shape and range from ~1 to 50 (rarely) cm in diameter; most are 5–10 cm. Most Tatoosh intrusive suite outcrops contain only a few enclaves per square meter, though along wall-rock contacts, especially at the east edge of the Stevens pluton in Stevens Canyon, enclaves are significantly more abundant. The enclaves are fine grained and composed of hypidiomorphic inequigranular to porphyritic intersertal intergrowths primarily composed of subhedral to euhedral plagioclase, anhedral clinopyroxene or hornblende, and Fe-Ti oxides. Euhedral plagioclase phenocrysts, 1–2 mm long, are a characteristic feature of Tatoosh intrusive suite enclaves. Clinopyroxene is replaced by hornblende in many enclaves, and hornblende is replaced by biotite in others; most hornblende is also altered to either tremolite-actinolite or chlorite. Anhedral interstitial quartz and alkali feldspar are volumetrically minor. A minor amount of anhedral to subhedral red brown biotite is also a constituent of all enclaves. Apatite and zircon, in varying abundances, are the accessory minerals present. Many Tatoosh intrusive suite enclaves contain centimeter-scale miarolitic cavities filled by quartz and chlorite, which indicate saturation with late-stage magmatic fluids. The shapes, chemical composition, and petrographic features of enclaves in Tatoosh intrusive suite plutons suggest that they, like enclaves in many igneous systems (Vernon, 1984), represent globules of mafic magma mingled with and quenched within more felsic magma; magma represented by the enclaves was sufficiently plastic that upon mingling, it formed disaggregated pillow structures in its host.

Quartz crystals in most Tatoosh intrusive suite pluton samples contain abundant fluid inclusions; crystallized melt inclusions are also present in some Tatoosh intrusive suite quartz (Item DR3 [see footnote 1]). Most fluid inclusions are ≤5–10 μm in maximum dimension, but some inclusions are as big as 25 μm. Most Tatoosh intrusive suite quartz crystals contain a myriad of healed fractures that host crosscutting planes of secondary fluid inclusions; few, if any, of the observed fluid inclusions are likely primary. At room temperature, Tatoosh intrusive suite pluton samples contain three types of fluid inclusions: liquid rich (type 1), vapor rich (type 2), and high salinity (type 3). Type 1 inclusions (least abundant) are two phase (liquid and vapor); vapor bubbles typically constitute ≤25% of inclusion volume, which is often irregularly shaped. Type 2 inclusions (most abundant) are vapor rich, and many consist of a large vapor bubble that completely fills the inclusion. Type 3 inclusions contain liquid, vapor, and one or more daughter crystals. Daughter crystals con-

sist of a square, colorless, isotropic phase inferred to be halite ± sylvite(?), hematite, and (or) several birefringent (high refractive index) minerals including a rhombic carbonate(?) mineral. Opaque daughter crystals, possibly including chalcopyrite, are rare.

WHOLE-ROCK CHEMICAL COMPOSITIONS

Major Oxide Data

Tatoosh intrusive suite pluton samples (exclusive of mafic enclave and dike samples) contain between ~59 and 71 wt% SiO_2, and the ranges (in wt%) of SiO_2 abundances (Table 2) in each of the three plutons, except the Reflection phase, are restricted: Pyramid (1%); Nisqually (full array, 5%; but excluding a single anomalously low SiO_2 sample, 3%), Stevens (full array, 4%; but excluding two anomalously high SiO_2 samples, 3%); and Reflection (7%). Common geochemical features (Figs. DR1–5 [see footnote 1]) of the Tatoosh intrusive suite plutons are consistent with their genesis in a continental margin arc setting. Relative to standard metrics (in cited sources), they are subalkaline (Irvine and Baragar, 1971), metaluminous (Shand, 1951), calc-alkaline (Miyashiro, 1974) and follow a calc-alkaline trend (Irvine and Baragar, 1971), magnesian (Frost et al., 2001), and transitional from calcic to calc-alkalic (Frost et al., 2001). On variation diagrams that define these char-

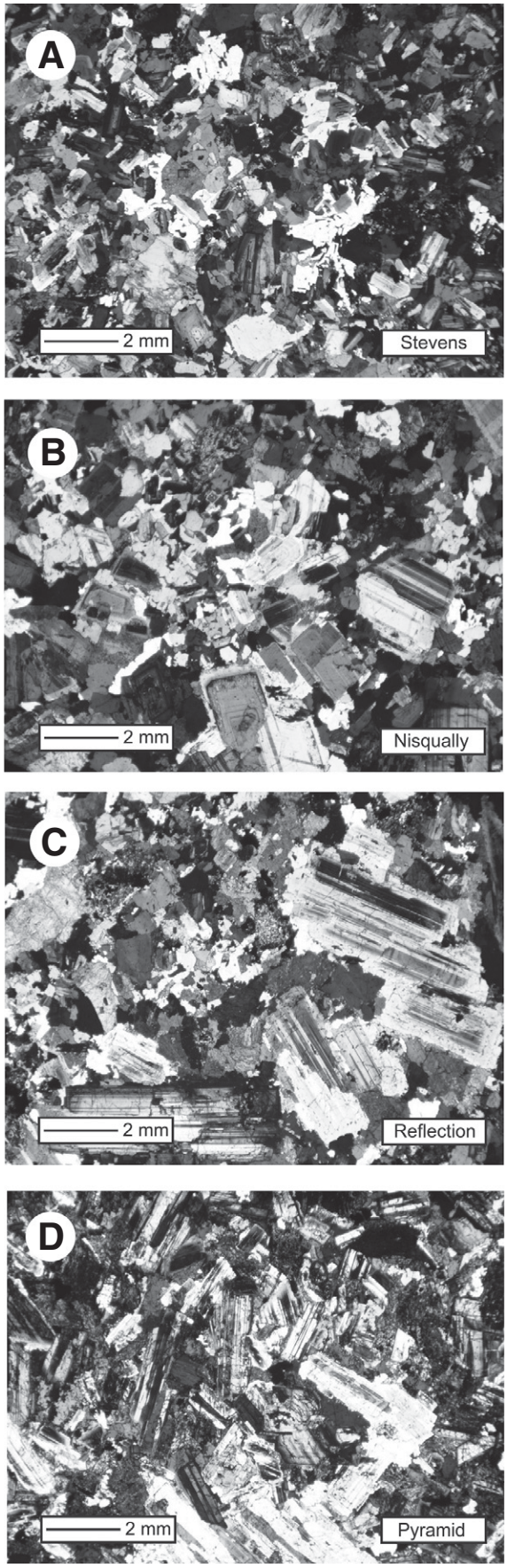

Figure 3. Low-magnification photomicrographs (crossed polarizers) showing characteristic compositions and textures of Tatoosh intrusive suite samples. (A) Fine-grained, seriate-textured Stevens pluton; contains biotite and minor clinopyroxene. Note 1–2 mm domains of quartz with micrographically intergrown alkali feldspar (granophyre) and relative dearth of large crystals. (B) Fine- to medium-grained, inequigranular Nisqually pluton; contains biotite and hornblende. Note 1–2 mm domains of quartz with micrographically intergrown alkali feldspar (granophyre); euhedral, oscillatory-zoned plagioclase; and low to moderate large crystal content. (C) Fine- to medium-grained, inequigranular Reflection phase; contains biotite and hornblende. Note subhedral, oscillatory-zoned plagioclase to 4 mm and moderate large crystal content. (D) Medium-grained, inequigranular Pyramid phase; contains hornblende and biotite. Note crystal-crowded, cumulate texture and relative scarcity of interstitial mesostasis.

acteristics, as well as on major oxide variation diagrams (Fig. 4), data for each Tatoosh intrusive suite pluton plot as a distinct compositional array. Approximately linear major oxide abundance variation arrays (Fig. 4) are characteristic of the Stevens and Nisqually plutons and Reflection phase; the few samples of the Pyramid phase suggest limited internal whole-rock geochemical variation. Major oxide arrays for most samples of the Stevens and Nisqually plutons define relatively minor within-pluton variation, whereas the compositional range of the Reflection phase is significantly greater. The Pyramid phase and the Stevens pluton are the least and most evolved, respectively. Major oxide contents of the Stevens and Nisqually plutons overlap slightly, but other geochemical features of these plutons, including total alkali content, Fe/Fe + Mg, and Al/Na + K are distinct. Weak hydrothermal alteration may have modified the primary compositions slightly, particularly alkali abundances. Reflection phase compositions overlap those of the Nisqually and Stevens plutons. Most Reflection phase compositions cluster with those for the least evolved samples of the Stevens pluton, whereas the remaining Reflection phase samples approach those of the Pyramid phase. Although compositions of the Tatoosh intrusive suite form semicontinuous arrays on SiO_2 versus major oxides plots, only five of 58 pluton samples have SiO_2 contents between 60 and 65% SiO_2 (Fig. 4). Concentrations of TiO_2, Al_2O_3, FeO*, MnO, MgO, CaO, and P_2O_5 decrease systematically with increasing SiO_2. Except for an overall decrease in Na_2O abundances with increasing SiO_2 in Stevens samples, Tatoosh intrusive suite rocks display no consistent covariation of Na_2O with SiO_2 content; and K_2O in each unit except Pyramid scatters to higher abundances with increasing SiO_2, with K_2O (and K/Na) being highest in Reflection, intermediate in Stevens, and low-

TABLE 2. REPRESENTATIVE COMPOSITIONS FOR SAMPLES OF TATOOSH INTRUSIVE SUITE CONSTITUENTS, MOUNT RAINIER NATIONAL PARK, WASHINGTON

Pluton/Phase:	Nisqually	Nisqually	Nisqually	Pyramid	Reflection	Reflection	Reflection	Stevens	Stevens	Stevens
Sample:	93T123	93T062	203081	203079	93T026	93T103	93T114	93T161	93T127	93T126
Lat 46°N	0.7914	0.7699	0.7922	0.7906	0.7647	0.7944	0.7781	0.7746	0.7709	0.7757
Long 121°W	0.7276	0.7341	0.7930	0.8073	0.7876	0.7262	0.7885	0.6730	0.6881	0.7011
SiO_2 (wt%)	63.66	66.03	68.39	58.96	60.14	65.47	67.48	66.89	68.80	71.22
TiO_2	0.80	0.67	0.55	1.06	1.00	0.90	0.73	0.68	0.57	0.49
Al_2O_3	16.17	15.36	15.29	17.34	16.41	15.35	14.93	15.39	14.87	14.22
FeO*	5.02	4.34	3.63	6.53	6.09	4.79	3.87	4.04	3.42	2.67
MnO	0.08	0.04	0.07	0.12	0.10	0.06	0.05	0.08	0.07	0.04
MgO	2.69	2.45	1.73	3.72	3.66	2.28	1.72	1.80	1.47	1.13
CaO	5.32	4.47	3.82	6.81	6.39	4.52	3.70	3.73	3.48	2.90
Na_2O	3.98	3.87	3.77	3.61	3.85	3.68	3.86	4.21	3.96	3.64
K_2O	2.13	2.64	2.61	1.63	2.16	2.78	3.51	3.06	3.27	3.62
P_2O_5	0.15	0.13	0.13	0.20	0.19	0.17	0.14	0.12	0.10	0.07
LOI	0.30	0.55	0.53	0.68	0.15	0.10	<0.01	0.85	0.50	0.40
$Total_i$	99.81	99.31	99.04	99.43	98.91	99.00	99.57	98.76	99.72	98.42
Sc (ppm)	11	10	9	16	16	11	9	8	7	6
V	91	77	69	151	149	84	81	74	52	45
Cr	30	20	20	50	70	20	20	20	10	<10
Co	15.0	11.7	10.0	19.1	22.3	10.5	10.0	10.1	8.3	5.8
Ni	24	23	10	11	38	15	11	10	8	5
Rb	58.6	71.4	71.7	48.4	75.7	83.9	116	93.9	102	96
Sr	398	363	311	418	400	331	259	322	315	266
Y	15.8	14.1	18.3	19.3	20.3	22.7	25.0	18.9	15.5	14.9
Zr	141	84	70.3	59.4	192	157	171	140	63.9	100
Nb	9	8	9	9	11	11	13	9	9	8
Li	20	20	30	<10	20	20	10	20	40	30
Cs	3.1	2.5	3.5	1.8	3.2	3.0	2.2	2.8	4.3	2.6
Ba	483	504	589	387	467	615	610	643	716	800
La	22.4	13.4	21.7	17.5	27.8	24.8	36.8	30.6	22.6	28.5
Ce	43.9	27.0	44.2	37.0	56.7	53.1	75.2	59.7	44.2	53.5
Pr	5.36	3.45	5.30	4.75	6.85	6.62	9.06	7.19	5.14	6.00
Nd	20.8	14.4	20.7	20.7	27.1	26.6	34.9	27.3	19.5	21.1
Sm	3.8	3.1	4.2	4.4	5.1	5.1	6.4	4.8	3.6	3.5
Eu	1.14	1.00	0.93	1.18	1.36	1.28	1.16	1.21	1.08	1.02
Gd	3.88	3.19	3.93	4.47	5.06	5.13	6.20	4.61	3.55	3.37
Tb	0.59	0.50	0.54	0.62	0.75	0.81	0.96	0.72	0.54	0.51
Dy	2.97	2.59	3.42	3.66	3.97	4.21	4.66	3.59	2.92	2.70
Ho	0.59	0.51	0.63	0.67	0.75	0.84	0.95	0.74	0.58	0.56
Tm	0.23	0.22	0.24	0.27	0.29	0.33	0.39	0.32	0.24	0.24
Yb	1.5	1.4	1.7	1.8	1.9	2.1	2.5	2.0	1.6	1.6
Lu	0.22	0.20	0.23	0.22	0.30	0.29	0.36	0.32	0.24	0.23
Hf	4	2	2	2	5	4	5	4	2	3
Ta	0.6	0.7	0.7	0.6	0.9	0.8	1.0	0.8	0.7	0.7
Cu	44	90	38	153	43	8	32	22	14	<5
Pb	10	8	10	14	28	15	10	16	12	22
Zn	82	43	58	121	85	52	47	81	65	63
Sn	2	6	1	4	3	2	2	33	2	4
Th	5.2	7.0	7.1	4.3	7.7	12.7	16.7	12.1	12.1	13.7
U	1.16	1.35	0.91	1.66	2.73	3.26	4.38	3.32	2.01	2.56
Ga	19	18	17	19	21	19	19	19	18	17

Note: Major oxides (recalculated to 100%, volatile free) are in weight percent; FeO* is total iron as FeO. $Total_i$ is prenormalization total. Trace elements are in parts per million. Ag (<1 ppm), As (<30 ppm), Be (<5 ppm), Bi (<0.01), Cd (<0.2 ppm), Ge (<1), In (<0.2 ppm), Mo (<2 ppm), Tl (<0.5 ppm), and W (<1 ppm) are below respective detection limits (values in parens) in most samples. LOI—loss on ignition.

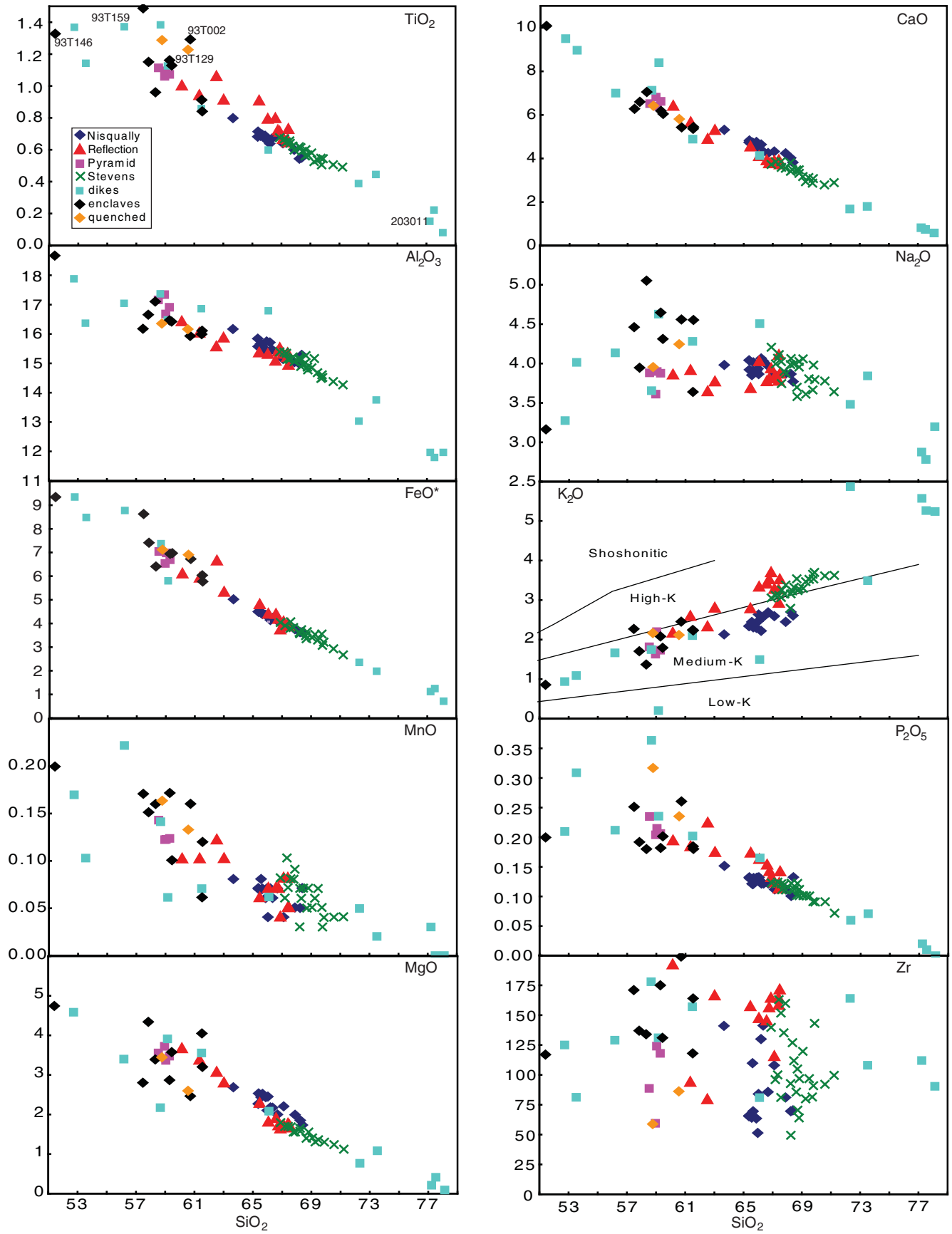

Figure 4. Variation diagrams showing abundances of major oxides (wt%) and zirconium (ppm) in Tatoosh intrusive suite samples. Field boundaries on K_2O versus SiO_2 diagram are from Le Maitre et al. (1989); high K-shoshonitic dividing line is from Ewart (1982).

est in Nisqually samples. Relative abundances of K_2O and SiO_2 in samples of each Tatoosh intrusive suite pluton are distinct (Fig. 4) and are transitional between medium- and high-K compositions (Gill, 1981).

Dikes and enclaves extend the Tatoosh intrusive suite spectrum to more mafic and more silicic compositions (Fig. 4; Table 3). The most felsic dikes (Fig. 4, 203011) are aplite, whereas the most mafic dikes are basaltic andesite. Some Tatoosh intrusive suite mafic enclaves appear variably hybridized (Fig. 4, 93T002), but one primitive (51% SiO_2) enclave (Fig. 4, 93T146) has a composition collinear with the Tatoosh intrusive suite compositional array. Other Tatoosh intrusive suite enclaves (Fig. 4, 93T002) have compositions similar to those of fine-grained rock (included in the Stevens pluton map unit) exposed on Mazama Ridge (Table 4).

Petrogenetic Implications of Major-Oxide Data

Dikes more evolved than Tatoosh intrusive suite plutons likely represent felsic magma, largely without entrained crystals, extracted as Tatoosh intrusive suite plutons solidified. Intergranular liquid (represented by mesostasis) separation can profoundly influence magma chemistry; its potential role in promoting chemical variation within each Tatoosh intrusive suite pluton was evaluated accordingly. Visually estimated melt fraction and point-count–determined quantities of quartz + alkali feldspar (which typically occur only as groundmass constituents) are strongly positively correlated (Fig. DR6 [see footnote 1]), which suggests that the quantity of quartz + alkali feldspar reflects the melt fraction in each Tatoosh intrusive suite sample. Similarly, major oxide abundance variations within each Tatoosh intrusive suite pluton correlate with apparent melt fraction. For exam-

TABLE 3. COMPOSITIONS OF DIKES (AND SILLS, SAMPLE 203014) ASSOCIATED WITH THE TATOOSH INTRUSIVE SUITE, MOUNT RAINIER NATIONAL PARK, WASHINGTON

Sample:	93T022	93T035	93T054	93T066	93T078	93T119	93T128	93T143	93T144	93T159	203011	203014
Lat 46°N	0.7908	0.7827	0.7580	0.7895	0.7886	0.7896	0.7709	0.7669	0.7669	0.7759	0.7704	0.7921
Long 121°W	0.7513	0.7614	0.7348	0.7138	0.7124	0.7237	0.6881	0.6702	0.6702	.6885	.6801	0.7457
SiO_2 (wt%)	78.13	77.52	73.52	59.16	61.49	53.53	72.32	58.67	52.73	56.18	77.23	66.10
TiO_2	0.08	0.22	0.44	1.13	0.86	1.14	0.39	1.38	1.37	1.37	0.15	0.60
Al_2O_3	11.97	11.79	13.75	16.48	16.86	16.37	13.03	17.37	17.88	17.04	11.97	16.79
FeO*	0.71	1.25	1.98	5.80	5.70	8.48	2.35	7.37	9.35	8.78	1.12	4.06
MnO	<0.01	0.00	0.02	0.06	0.07	0.10	0.05	0.14	0.17	0.22	0.03	0.06
MgO	0.09	0.41	1.08	3.91	3.55	6.00	0.77	2.17	4.58	3.40	0.21	2.08
CaO	0.58	0.75	1.80	8.39	4.89	8.97	1.68	7.13	9.50	7.00	0.82	4.14
Na_2O	3.20	2.78	3.84	4.63	4.28	4.01	3.48	3.66	3.28	4.14	2.88	4.51
K_2O	5.24	5.26	3.49	0.20	2.10	1.09	5.87	1.75	0.94	1.66	5.57	1.50
P_2O_5	<0.01	0.01	0.07	0.24	0.20	0.31	0.06	0.36	0.21	0.21	0.02	0.16
LOI	0.26	0.25	0.75	0.55	0.52	0.35	0.05	0.10	<0.01	0.33	0.3	2.30
$Total_i$	99.79	99.59	99.86	98.88	100.20	98.42	100.80	99.94	101.20	100.50	99.87	99.27
Sc (ppm)	<5	<5	<5	16	11	21	<5	18	28	22	<5	7
V	12	15	43	130	153	190	39	104	283	221	17	63
Cr	<10	<10	<10	30	80	110	<10	<10	50	10	<10	<10
Co	1.4	2.5	3.4	17.2	27.9	23.5	5.4	13.9	32.9	22.2	2.9	9.8
Ni	9	<5	29	16	31	58	12	<5	16	6	10	14
Rb	82.9	86.3	79.8	2.6	125	45.9	199	43.3	22.3	63.7	146	30.7
Sr	54.2	119	230	431	388	927	130	457	459	365	126	371
Y	2.3	4.9	13.0	38.3	9.2	19.9	28.6	34.2	27.0	28.2	12.5	8.3
Zr	90.4	56.3	108	131	157	81.2	164	178	125	129	112	80.9
Nb	<1	5	8	12	7	5	13	14	8	8	5	6
Li	<10	20	20	<10	30	30	20	20	20	20	30	70
Cs	1.3	1.6	1.6	0.2	10.1	2.8	5.0	1.3	1.6	3.3	3.3	2.1
Ba	215	1030	1050	79	211	294	316	456	286	352	441	411
La	29.2	15.5	22.7	13.2	12.7	38.2	45.3	23.7	15.5	17.6	46.8	16.1
Ce	44.2	25.6	42.8	39.8	23.7	98.3	86.9	51.1	33.1	41.4	88.5	31.1
Pr	4.05	2.56	4.72	6.38	2.91	13.20	9.77	7.01	4.64	5.89	9.92	4.08
Nd	10.7	8.4	16.5	29.7	10.9	53.5	32.7	29.7	19.0	23.8	32.2	15.2
Sm	1.2	1.2	2.8	7.4	2.4	8.8	6.1	6.5	4.7	5.4	5.0	2.9
Eu	0.40	0.60	0.77	1.37	0.69	2.74	0.56	2.16	1.47	1.38	0.61	0.99
Gd	0.88	1.07	2.70	8.32	2.30	7.58	5.86	7.17	5.14	5.77	3.66	2.70
Tb	0.12	0.15	0.44	1.32	0.32	1.00	0.89	1.20	0.83	0.96	0.48	0.41
Dy	0.39	0.76	2.28	7.41	1.58	4.40	4.80	6.34	4.75	5.31	2.17	1.80
Ho	0.08	0.16	0.46	1.45	0.34	0.84	1.01	1.34	1.05	1.08	0.43	0.35
Tm	<0.05	0.08	0.21	0.59	0.13	0.28	0.47	0.57	0.44	0.44	0.21	0.11
Yb	0.4	0.5	1.3	3.6	0.9	1.9	3.2	3.4	2.7	2.9	1.5	0.8
Lu	0.09	0.08	0.18	0.55	0.22	0.26	0.55	0.54	0.43	0.46	0.25	0.13
Hf	4	2	3	4	4	3	6	4	3	3	5	3
Ta	<0.5	0.7	0.9	0.7	<0.5	<0.5	1.3	1.0	<0.5	<0.5	0.9	<0.5
Cu	20	15	<5	8	8	266	24	23	71	38	14	26
Pb	12	15	16	<5	22	<5	35	9	13	12	17	7
Zn	14	24	39	32	89	70	34	83	98	116	49	62
Sn	<1	<1	3	6	7	11	2	2	<1	2	<1	<1
Th	28.1	11.0	16.3	6.5	6.4	6.9	36.4	4.3	3.6	4.2	26.5	2.1
U	2.98	1.54	4.09	2.43	2.15	2.96	5.22	1.45	1.14	1.82	5.48	0.73
Ga	13	13	15	20	24	20	18	22	23	24	15	18

Note: Major oxides (recalculated to 100%, volatile free) are in weight percent; FeO* is total iron as FeO. $Total_i$ is prenormalization total. Trace elements are in parts per million. Ag (<1 ppm), As (<30 ppm), Be (<5 ppm), Bi (<0.01), Cd (<0.2 ppm), Ge (<1), In (<0.2 ppm), Mo (<2 ppm), Tl (<0.5 ppm), and W (<1 ppm) are below respective detection limits (values in parens) in most samples.

ple, FeO* abundances (Fig. 5A) are negatively correlated with melt fraction, whereas K_2O abundances (Fig. 5B) are positively correlated. Consequently, variable crystal content, probably a consequence of variable melt extraction, is strongly associated with major oxide compositional variation within Tatoosh intrusive suite plutons. Bachl et al. (2001), Harper et al. (2004), and Walker et al. (2007) have also suggested a major role for variable melt segregation in development of compositional variability within similar magmatic systems.

Least squares multiple regression was used to further evaluate melt extraction as a cause for compositional variation within each Tatoosh intrusive suite pluton (Table 5). Melt extraction yields an evolved silicate liquid available for reinjection as dikes or eruption and a more primitive derivative magmatic component of crystals plus trapped liquid (orthocumulate). For modeling purposes, the composition of a representative Tatoosh intrusive suite aplite dike (sample 203011) was selected to represent mesostasis compositions. To test the intergranular liquid extraction hypothesis, we selected a representative, more evolved sample from the data cluster for each Tatoosh intrusive suite pluton as its initial composition (mixing end members and pathways graphically identified on Fig. 5). Evaluated mixing models have the form:

Initial composition minus melt (aplite) = composition of more mafic cumulate sample. Models were run to evaluate derivation of the most primitive sample of the Nisqually and Stevens plutons and Reflection phase from their

TABLE 4. COMPOSITIONS OF MAFIC ENCLAVES AND FINE-GRAINED, QUENCHED VARIANT OF THE STEVENS PLUTON, TATOOSH INTRUSIVE SUITE, MOUNT RAINIER NATIONAL PARK, WASHINGTON

Sample:	Enclave 93T002	Enclave 93T025*	Enclave 93T050	Enclave 93T129	Enclave 93T130	Enclave 93T133	Enclave 93T146	Enclave 203012B	Enclave 203013B	Quenched† 93T012	Quenched† 203082
Lat 46°N	0.7552	0.7908	0.7562	0.7709	0.7709	0.7709	0.7669	0.7886	0.7891	0.7881	0.7882
Long 121°W	0.6996	0.7513	0.7342	0.6881	0.6881	0.6881	0.6706	0.7129	0.7128	0.7083	0.7111
SiO_2 (wt%)	60.72	61.54	61.51	59.30	58.32	57.47	51.41	59.45	57.84	60.56	58.77
TiO_2	1.29	0.84	0.91	1.16	0.96	1.49	1.33	1.13	1.15	1.23	1.29
Al_2O_3	15.93	16.11	15.99	16.47	17.11	16.18	18.67	16.42	16.66	16.16	16.35
FeO*	6.73	5.77	6.04	6.94	6.41	8.63	9.34	6.97	7.41	6.91	7.12
MnO	0.16	0.12	0.06	0.17	0.16	0.17	0.20	0.10	0.15	0.13	0.16
MgO	2.46	3.20	4.05	2.87	3.39	2.80	4.74	3.58	4.34	2.60	3.44
CaO	5.43	5.44	5.36	6.18	7.05	6.28	10.08	6.05	6.60	5.81	6.42
Na_2O	4.56	4.55	3.64	4.65	5.05	4.46	3.16	4.31	3.95	4.25	3.96
K_2O	2.45	2.23	2.25	2.08	1.37	2.27	0.86	1.79	1.71	2.12	2.17
P_2O_5	0.26	0.18	0.18	0.18	0.18	0.25	0.20	0.20	0.19	0.24	0.32
LOI	0.31	0.42	0.70	0.21	0.28	0.38	<0.01	0.6	0.57	0.10	0.40
$total_i$	100.90	101.00	98.90	99.97	101.00	100.90	101.20	100.60	100.50	98.60	99.01
Sc (ppm)	16	16	15	19	20	19	28	17	19	16	18
V	143	119	142	146	113	196	267	154	166	142	119
Cr	10	50	100	10	40	<10	50	80	100	<10	40
Co	16.8	19.4	17.7	16.9	19.7	18.2	33.2	24.3	29.1	17.4	14.4
Ni	17	36	56	16	20	14	10	34	43	5	60
Rb	75.1	60.2	98.2	60.7	39.6	73.7	17.7	71.8	66.8	54.2	47.8
Sr	254	248	324	269	273	253	509	307	336	361	515
Y	39.9	28.7	16.9	33.8	28.7	35.0	24.7	23.7	19.0	21.3	22.1
Zr	199	164	118	175	134	171	117	131	137	86.2	58.8
Nb	17	12	9	19	14	18	8	11	8	10	7
Li	30	<10	50	20	20	20	20	20	30	20	<10
Cs	3.6	2.4	6.8	3.1	8.1	6.5	1.6	3.2	5.6	1.5	3.2
Ba	427	385	328	395	277	298	265	326	333	574	651
La	30.0	29.4	21.4	25.6	25.6	27.1	14.4	24.5	19.6	22.3	30.1
Ce	64.5	63.5	43.6	54.1	50.1	58.8	30.4	54.8	40.3	45.8	61.1
Pr	8.80	8.29	5.25	7.25	6.51	8.03	4.17	7.22	5.18	5.71	8.19
Nd	35.5	32.4	20.9	28.8	25.8	32.2	17.5	27.4	19.5	23.3	33.5
Sm	8.4	6.9	4.0	6.8	6.0	7.4	4.3	5.6	4.1	4.6	7.1
Eu	1.12	1.28	1.13	1.16	1.21	1.09	1.33	1.43	1.21	1.47	1.74
Gd	8.30	6.51	4.10	6.89	6.01	7.63	4.96	5.60	4.45	4.84	6.24
Tb	1.36	1.04	0.63	1.09	0.96	1.21	0.77	0.85	0.68	0.79	0.83
Dy	7.27	5.43	3.28	6.00	5.38	6.60	4.40	4.51	3.64	3.94	4.59
Ho	1.52	1.10	0.64	1.26	1.07	1.35	0.99	0.93	0.75	0.78	0.78
Tm	0.59	0.44	0.28	0.51	0.45	0.56	0.42	0.35	0.28	0.32	0.29
Yb	3.7	2.9	1.6	3.2	2.7	3.6	2.6	2.2	1.9	2.0	2.1
Lu	0.54	0.45	0.24	0.53	0.45	0.61	0.43	0.45	0.33	0.29	0.26
Hf	5	5	3	5	4	4	3	4	4	3	2
Ta	0.9	0.7	0.7	1.0	0.6	0.8	<0.5	0.5	<0.5	0.7	<0.5
Cu	59	46	9	109	17	94	92	7	182	40	96
Pb	17	10	14	46	44	45	7	15	36	11	18
Zn	137	83	38	133	156	123	96	64	91	51	77
Sn	1	<1	9	2	<1	2	<1	4	<1	3	2
Th	9.8	9.1	7.2	12.1	7.5	11.2	3.3	8.7	6.4	6.9	5.7
U	3.74	1.47	2.34	2.41	2.56	2.24	1.07	2.02	1.47	1.64	1.44
Ga	23	21	20	22	23	24	23	21	21	20	17

Note: Major oxides (recalculated to 100%, volatile free) are in weight percent; FeO* is total iron as FeO. $Total_i$ is prenormalization total. Trace elements are in parts per million. Ag (<1 ppm), As (<30 ppm), Be (<5 ppm), Bi (<0.01), Cd (<0.2 ppm), Ge (<1), In (<0.2 ppm), Mo (<2 ppm), Tl (<0.5 ppm), and W (<1 ppm) are below respective detection limits (values in parens) in most samples.

*Sample 93T025 is an enclave from the Nisqually pluton.

†Quenched roof zone of Stevens pluton on Mazama Ridge.

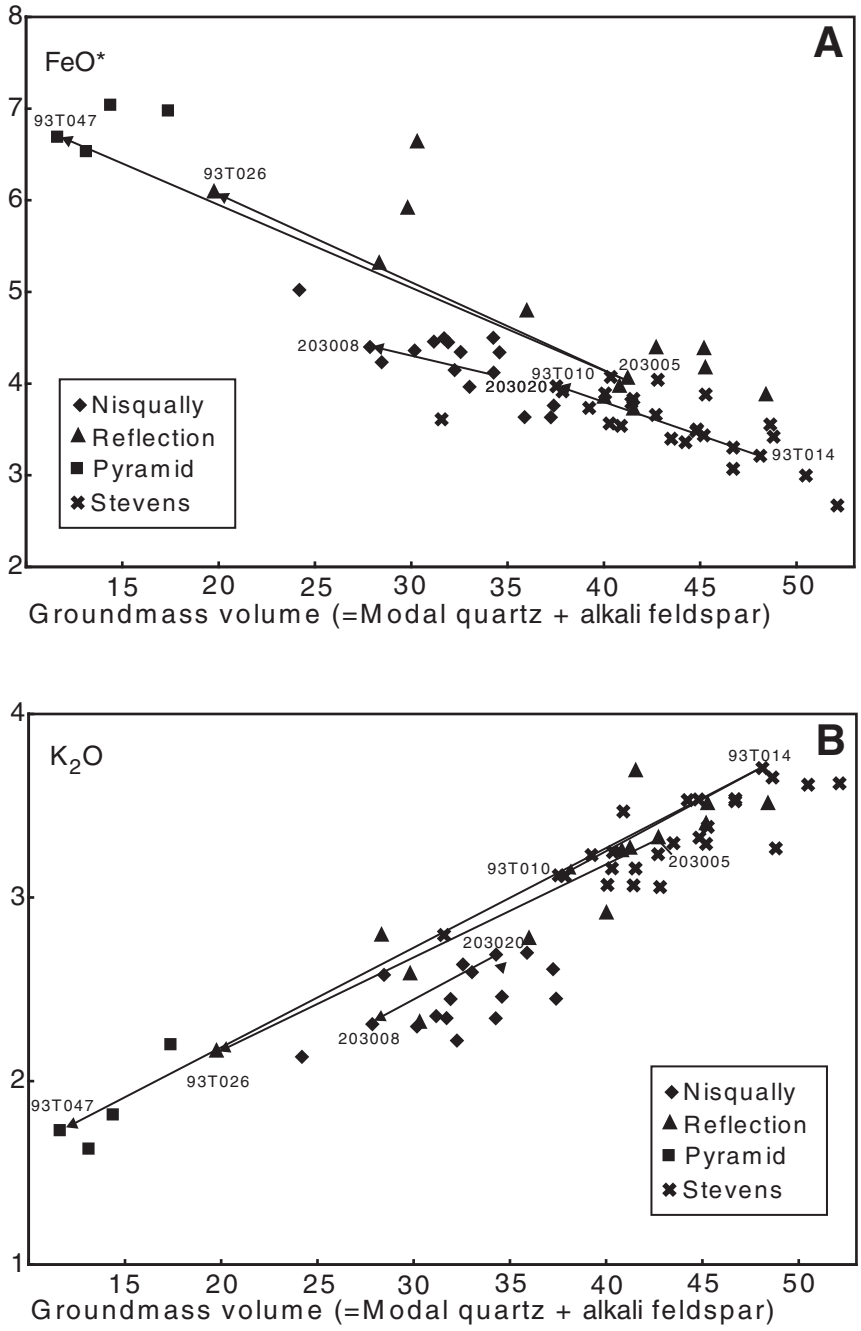

Figure 5. Variation diagrams showing weight percent of major oxides relative to groundmass volume percent for Tatoosh intrusive suite samples. Rays define mixing model pathways (Table 5); samples at arrow heads and at arrow bases are derived and initial compositions, respectively. (A) FeO* versus groundmass. (B) K_2O versus groundmass.

TABLE 5. RESULTS OF MAJOR-OXIDE LEAST SQUARES MIXING MODELS FOR PLUTONS OF THE TATOOSH INTRUSIVE SUITE, MOUNT RAINIER NATIONAL PARK, WASHINGTON

	Initial	*minus*	Aplite	*equals*	Cumulate	
	Sample no.	Mass fraction	Sample no.	Mass fraction	Sample no.	Mass fraction	Residual
Stevens	93T014	1.000	203011	0.247	93T010	0.753	0.026
Nisqually	203020	1.000	203011	0.092	203008	0.908	0.152
Reflection	203005	1.000	203011	0.405	93T026	0.595	1.064
Pyramid	203005	1.000	203011	0.436	93T047	0.564	0.672

Note: For example, extraction of a liquid (having the composition of aplite 201011) aliquot equal to 24.7%, the mass of an inferred initial composition, represented by 93T014, yields a cumulate aliquot having a mass 75.3% of the initial composition. Data in the residual column are the sum of the squares of oxide residuals for the calculated initial composition relative to the actual initial composition.

more evolved, presumed initial compositions by melt extraction. Because the Pyramid phase is thought to be composed essentially of accumulated crystals similar to and derived from those characteristic of the Reflection phase, its internal compositional variation was evaluated for the possibility that Pyramid samples depict end-stage residuum resulting from significant melt extraction from a presumed initial Reflection composition. Compositional similarities between Pyramid and Reflection plagioclase crystals further support the hypothesis that the Pyramid phase is largely composed of an accumulation of crystals derived from the Reflection phase (Item DR4, Table DR4, and Figs. DR 7–9 [see footnote 1]).

Derivation of the most primitive Stevens and Nisqually compositions from presumed initial compositions requires only moderate (10%–25%) melt extraction; very small associated residuals support the suitability of the proposed models. In contrast, derivation of the most primitive Reflection composition from its presumed initial composition requires substantial (40%) melt extraction. Although the calculated residual for this mixing model is larger (Table 5), relatively low observed Reflection mesostasis abundances are in accord with the large calculated mass of extracted melt. Similarly, derivation of the least evolved Pyramid composition from the Reflection initial composition requires a large amount of melt extraction, but cumulate textures and the very small mesostasis volume characteristic of the Pyramid phase are consistent with calculated results. In all cases, these calculations address extreme, end-member evolutionary scenarios; derivation of numerous, less primitive compositions from presumed initial compositions requires significantly smaller amounts of melt extraction. The largest modeled extracted melt volumes are inconsistent with the relatively low abundance of aplite dikes within the Tatoosh intrusive suite and suggest that some extracted melt may have been transported to a shallower level and possibly erupted as rhyolite.

Crystallization differentiation (crystal-liquid fractionation) was responsible for the compositional evolution characteristic of the Tatoosh intrusive suite plutons. However, the Tatoosh intrusive suite rocks are not interpreted as series of derivative liquids from which crystals had settled, or otherwise had been mechanically removed, and that subsequently crystallized more-or-less in situ. Compositional evolution via intergranular liquid extraction and separation of non-groundmass crystals from magma represent the same crystallization-differentiation process viewed from contrasting end points. The question "in which direction did the process operate?" is largely answered by petrographic characteristics of Tatoosh intrusive suite rocks. The chemically least evolved part of each pluton has the highest crystal content and is cumulate textured. Derivation of more evolved pluton sample compositions from magma with bulk compositions of these crystal-rich rocks seems implausible because of the large magnitude of crystal removal required. Separation of intergranular liquid from a relatively evolved magma, resulting in a geochemically more primitive, crystal-enriched cumulate and a more evolved derivative liquid that escaped to be erupted or reinjected into superjacent crystal mush, seems to be the best explanation for the compositional evolution and petrographic characteristics of Tatoosh intrusive suite plutons.

The wide array of Reflection phase compositions, intermediate between those of the Pyramid phase and Nisqually or Stevens plutons, suggests that Reflection phase compositions result from mixing between magmas represented by the Pyramid phase and those represented by the Nisqually and (or) Stevens plutons. However, distinctive fabric and texture characteristics of each of these plutons and the absence of macroscopically observable mixing or mingling features within the Reflection phase invalidate mixing as a cause for its compositional variation. Subtle, off-trend compositional arrays (relative to compositional arrays for other Tatoosh intrusive suite plutons) characteristic of the Reflection phase (Fig. 4; Table DR2 [see footnote 1]), including slightly elevated abundances of TiO_2, K_2O, and P_2O_5 and slightly low abundances of Al_2O_3 and CaO, distinguish its composition and further suggest that magma mixing was not responsible for compositional variation within the Reflection phase.

Trace-Element Data

Trace-element abundances for the Tatoosh intrusive suite define characteristic ranges diagnostic of each pluton. In addition, primitive mantle–normalized extended trace-element patterns (Item DR5 and Fig. DR10 [see footnote 1]) for plutons of the Tatoosh intrusive suite have high large ion lithophile element (LILE) abundances and low high field strength element (HFSE) abundances, similar to those of other convergent margin, broadly calc-alkaline igneous rocks (Item DR5 [see footnote 1]), such as those in the Andean, Kamchatka, and Central American arcs (GEOROC, 2007). Relative trace-element abundance tectonic classification schemes, including Rb versus Y + Nb (Fig. DR11 [see footnote 1]) of Pearce et al. (1984), are consistent with Tatoosh intrusive suite pluton origins in a convergent margin (magmatic arc) environment. Tatoosh intrusive suite genesis in a magmatic arc setting is further corroborated by values of incompatible trace-element ratios. Wood et al. (1979) and Gill (1981) established that Ba/Ta, Ba/Nb, and La/Nb ratios for modern arc rocks are >450, >26, and 2–7, respectively. Average Ba/Ta, Ba/Nb, and La/Nb ratios for all Tatoosh intrusive suite samples are 830, 74, and 3 (Table DR2 [see footnote 1]), respectively. Importantly, each Tatoosh intrusive suite pluton is also characterized by relatively distinctive ranges of values for each of these trace-element parameters (Table DR2, Figs. DR12–14 [see footnote 1]). In evolving magmatic systems influenced by plagioclase separation, melt compositions become relatively Sr depleted and K enriched with differentiation. In contrast, Tatoosh intrusive suite rocks represent the complement to melt evolution. Relatively K-enriched, Sr-depleted initial bulk magma compositions produced relatively K-depleted and Sr-enriched rocks by variable loss of evolved interstitial melt (Fig. DR15 [see footnote 1]).

Abundances of compatible elements Co, Cr, Ni, Sc, and V decrease with increasing SiO_2, whereas abundances of Ba and Th increase (Figs. DR16–22 [see footnote 1]). Among the Tatoosh intrusive suite plutons, Cu and SiO_2 abundances display no consistent covariation, and Cu abundances in most Stevens pluton samples are low relative to those in other Tatoosh intrusive suite plutons (Fig. DR23 [see footnote 1]).

Chondrite-normalized rare earth element (REE) patterns for the Tatoosh intrusive suite are typical of intermediate composition, calc-alkaline continental margin magmatic arc igneous rocks (e.g., Gill, 1981; Cameron and Cameron, 1985; Wark, 1991; Feeley and Davidson, 1994). REE patterns have negative slopes and moderate negative Eu anomalies (Fig. 6); light REE (LREE) pattern segments have somewhat steeper slopes than heavy REE (HREE) segments. Reflection phase samples have the highest overall REE contents; Nisqually pluton samples have the lowest. Within each Tatoosh intrusive suite pluton, REE abundances vary within restricted ranges and have similar-magnitude negative Eu anomalies, REE patterns are mostly subparallel (La_N/Yb_N values define narrow ranges), and the magnitude of negative Eu anomalies tends to increase (Eu/Eu* decreases) with increasing REE concentrations (Fig. 6; Item DR6 and Table DR5 [see footnote 1]).

Tatoosh intrusive suite dikes have a wide range of trace-element abundances (Table 3; Fig. 6E). Chondrite-normalized REE patterns for aplite dikes are especially diverse (Fig. DR24 [see footnote 1]). These dikes have negatively sloping patterns, especially steep in their LREE segments, and are nearly flat in their HREE

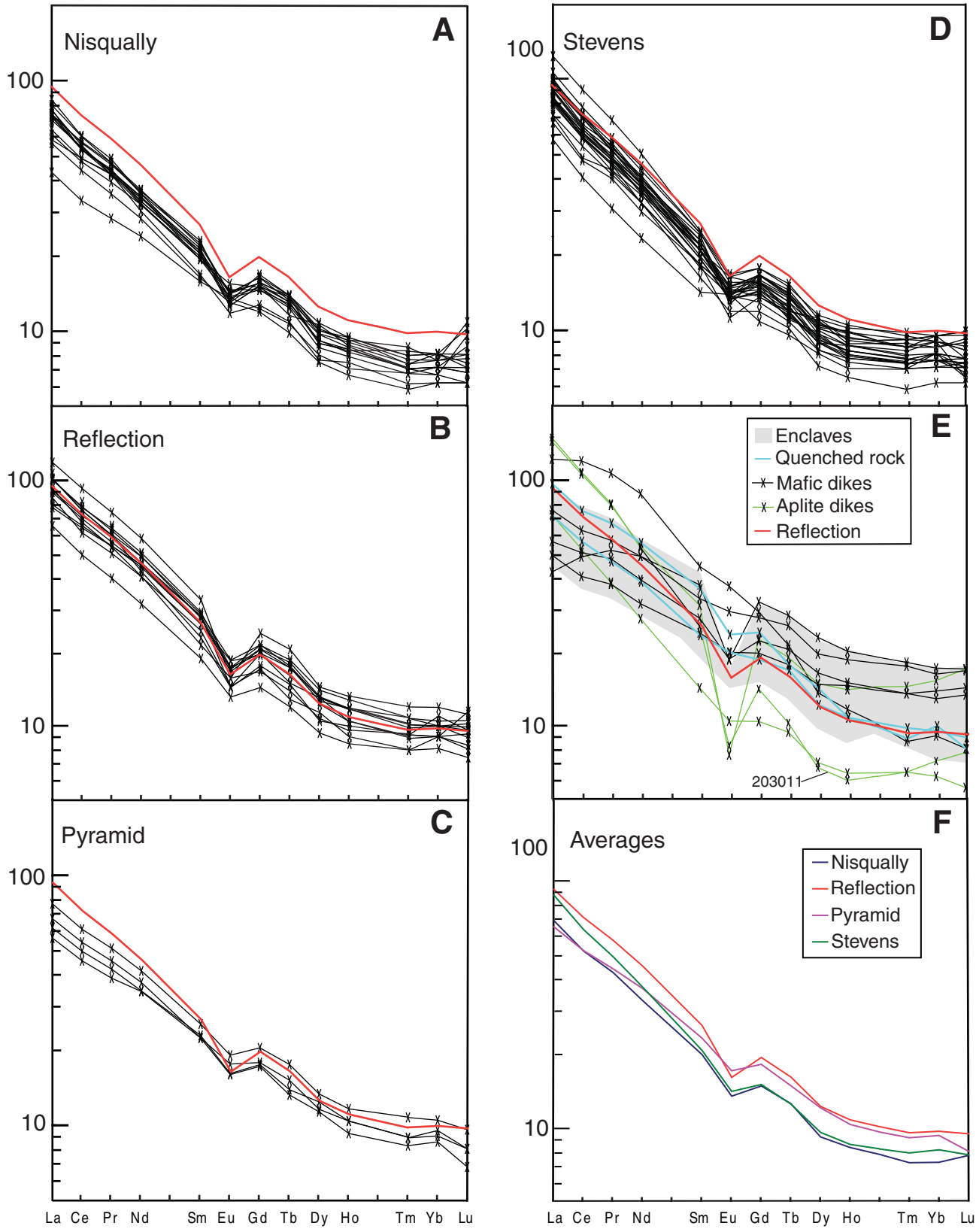

Figure 6. Chondrite-normalized rare earth element (REE) diagrams for Tatoosh intrusive suite samples; chondrite abundances are from Anders and Ebihara (1982). Average pattern for the Reflection phase is shown (in red) for reference. (A) Nisqually pluton. (B) Reflection phase. (C) Pyramid phase. (D) Stevens pluton. (E) Enclaves (gray field encloses REE patterns for nine enclave samples), quenched rock, and representative dikes. (F) Averages.

segments. Patterns for two aplite dikes have significant negative Eu anomalies, two have no Eu anomaly, and one has a small positive Eu anomaly. The pattern for a representative aplite dike (203011, Fig. 6E) has a fairly steep negatively sloped LREE segment, a well-developed negative Eu anomaly (Eu/Eu* = 0.42), and flat to U-shaped HREE segment. Chondrite-normalized REE patterns for mafic dikes associated with the Tatoosh intrusive suite are more systematic and clustered than those for the aplite dikes (Fig. DR24 [see footnote 1]). These patterns are continuously, moderately negatively sloping and, excluding one dike, lack significant negative Eu anomalies. REE patterns for Tatoosh intrusive suite mafic enclaves form a fairly cohesive cluster (Fig. 6E). Patterns are gently negatively sloping and most include well-developed negative Eu anomalies (representative sample 93T129, Eu/Eu* = 0.51). Notably, LREE abundances for representative mafic enclaves are similar to those of Tatoosh intrusive suite plutons, but the enclaves have larger negative Eu anomalies and higher HREE abundances (Fig. 6).

Petrogenetic Implications of Trace-Element Data

The viability of the melt extraction hypothesis was further investigated using trace-element systematics. Trace-element abundances were regressed against the quantity quartz + alkali feldspar in order to determine trace-element abundances at 100% quartz + alkali feldspar (presumably the composition of extracted melt) and compared to the composition of the representative aplite dike (203011). Abundances of Sr, Eu, and Th, in particular, predicted by regression are similar to representative aplite abundances. These data support the hypothesis that less silicic, more primitive samples within each pluton evolved from initial Tatoosh intrusive suite magma compositions, approximated by the more evolved, silicic samples of each pluton, via variable amounts of intergranular liquid melt extraction and crystal cargo accumulation.

Two samples (93T012 and 203082) of quenched Stevens pluton have Cu contents 2–5 times greater than those of other Stevens samples (Table DR2 [see footnote 1]) and may preserve initial Stevens pluton Cu abundances. Relatively large mesostasis volumes and distinctive porphyry textures characteristic of the Stevens pluton are consistent with smaller amounts of crystallization prior to a final burst of H_2O-rich vapor exsolution and rapid pressure-quench crystallization, compared to the other Tatoosh intrusive suite plutons. If the Stevens magma was vapor saturated, or H_2O-rich vapor saturation occurred relatively early during crystallization of the Stevens pluton, Cu was likely preferentially partitioned from the magma into a vapor phase, which mediated its loss from the system (Simon et al., 2006) during passive degassing; this accounts for differing Cu abundances in normal Stevens pluton and its quenched variant. Higher Cu abundances in other Tatoosh intrusive suite plutons that have lower mesostasis fractions, diagnostic of more advanced crystallization, suggest Cu retention in early formed minerals. For example, notably large Cu abundances in Pyramid phase samples likely reflect its incorporation and retention in early crystallized pyrrhotite.

Relatively low REE abundances in the Stevens pluton, which is otherwise more evolved than the other plutons, could reflect differences in parental magmas or combined effects of zircon + apatite ± allanite ± titanite separation (Hanson, 1980); allanite and titanite are present in some Stevens pluton samples but rare in other Tatoosh intrusive suite pluton samples. Relatively low LREE and small negative Eu anomalies characteristic of the Pyramid phase may reflect plagioclase accumulation, whereas higher HREE concentrations may reflect amphibole ± pyroxene ± zircon accumulation. The overall similarity of Tatoosh intrusive suite pluton REE abundances (Fig. 6; Table DR5 [see footnote 1]) suggests that these plutons originated and evolved via similar magmatic processes.

Relatively small negative Eu anomalies characteristic of the Tatoosh intrusive suite plutons invite an explanation involving relatively oxidized magma. However, oxidizing conditions that would have favored Eu^{3+} seem unlikely given the presence of ilmenite and relative scarcity of magmatic titanite in most Tatoosh intrusive suite rocks. Mafic enclaves presumed to represent parental compositions have more well-developed negative Eu anomalies (as well as higher total REE contents). Importantly, the negative Eu anomaly of the representative (sample 203011) Tatoosh intrusive suite aplite dike (mesostasis proxy) is significantly larger than anomalies typical of the Tatoosh intrusive suite plutons (Fig. 6E). Therefore, melt extraction would yield a crystal-enriched residuum with a smaller negative Eu anomaly than that of parental magmas, such as represented by enclaves. The Pyramid phase, which has the smallest negative Eu anomaly and demonstrably cumulate textures, lost the greatest amount of melt and is a crystal cumulate.

Although REE patterns for the three Tatoosh intrusive suite plutons are subparallel, patterns for the Pyramid phase are subtly rotated counterclockwise relative to those of the Stevens and Nisqually plutons (Fig. 6). REE patterns for the Pyramid phase could have evolved from patterns like those of the Reflection phase by removal (from the Reflection) of a component with a slightly more steeply negatively sloped REE pattern. The REE pattern for the representative (203011) aplite dike (residual melt proxy) has these characteristics. Similarly, more subtle within-pluton REE pattern rotation may reflect variable melt extraction among samples of a given Tatoosh intrusive suite pluton.

Relative trace-element concentrations indicate a comparatively limited role for two-component magma mixing as a cause of compositional variation within plutons of the Tatoosh intrusive suite. Magma mixing should yield a linear array, the end point and intermediate compositions of which are inferred initial and derived compositions, respectively. However, Tatoosh intrusive suite pluton trace-element abundances (Fig. DR25 [see footnote 1]) do not generally form the linear arrays characteristic of magma mixing. In addition, incompatible-element concentration scatter (e.g., Fig. 4, Zr vs. SiO_2) is inconsistent with two-component magma mixing. Because compositional effects of mixing and unmixing are described by similar mathematical expressions, an unmixing compositional array should also be linear. However, the physical mechanics of unmixing, including variably complete separation of crystals and liquid, as well as potential entrainment of locally distinct crystal species, are more likely than mixing to yield nonlinear compositional arrays similar to those characteristic of Tatoosh intrusive suite plutons. Other trace-element abundances (Fig. DR26 [see footnote 1]) form linear arrays for individual Tatoosh intrusive suite plutons, but these arrays are offset with respect to one another. Consequently, the compositions of the Tatoosh intrusive suite plutons as a group are also inconsistent with a magma mixing origin. These relationships consign simple two-component magma mixing to at most a second-order process relative to Tatoosh intrusive suite rock compositional variation.

In contrast to most other constituents, Zr abundances are highly variable within each of the Tatoosh intrusive suite plutons (Figs. 4; Figs. DR10 and DR27 [see footnote 1]). Incompatible behavior causes Zr abundances to increase systematically with increasing whole-rock SiO_2 until zircon saturation is achieved (Watson, 1979), a relationship exemplified by most other ancestral Cascades arc rocks (du Bray et al., 2006). In contrast, Tatoosh intrusive suite pluton Zr abundances vary inconsistently relative to SiO_2. In Tatoosh intrusive suite samples, variable Zr abundances are not correlated (Fig. DR28 [see footnote 1]) with modal quartz + alkali feldspar (mesostasis volume proxy). Physical separation of zircon, incorporated into

extracted residual liquid in variable amounts, is most consistent with erratic whole-rock Zr concentrations.

Whole-Rock Isotopic Data

Reconnaissance radiogenic and stable isotope data (Table 6) for samples of each of the Tatoosh intrusive suite plutons are similar to values for other igneous rocks for which genesis is commonly ascribed to arc magmatism including a significant mantle component. Although isotopic data for the three plutons are grossly similar, they are sufficiently distinct that derivation of each pluton from a distinct magma batch seems likely. The anomalously low $\delta^{18}O$ value for the Stevens pluton sample is the single most distinctive isotopic characteristic available for the Tatoosh intrusive suite plutons. Given that the Stevens pluton is the oldest of the Tatoosh intrusive suite plutons, is the only Tatoosh intrusive suite pluton demonstrably in contact with older wall and roof rocks, and, in some places near wall and roof rock contacts, contains abundant fragments of the enclosing rocks, assimilation of older, previously altered wall rock may be partly responsible for its distinctive $\delta^{18}O$ composition. However, the sample also contains secondary biotite and sodic-altered plagioclase that are consistent with weak hydrothermal alteration. Consequently, subsolidus exchange with isotopically light hydrothermal fluid may also have contributed to the low $\delta^{18}O$ value. Intrusion of the Stevens pluton may have limited access of later emplaced Tatoosh intrusive suite plutons to meteoric hydrothermal fluid and allowed their $\delta^{18}O$ compositions to retain a magmatic character.

ZIRCON U-Pb AGES

The primary goal in obtaining secondary ion mass spectrometry (SIMS) U-Pb geochronologic data for zircon in Tatoosh intrusive suite samples was to determine solidification ages of samples from plutons defined on the basis of field relationships, petrography, and geochemistry and establish the duration of the Tatoosh intrusive suite magmatic event. A secondary goal was to discover if zircon had been inherited from basement rocks (xenocrysts) or recycled from earlier crystallization events associated with the Miocene Tatoosh intrusive suite (antecrysts). Tatoosh intrusive suite zircons consist of cores (central parts of grains), rims (the array of fine, concentric, lamellar growth zones surrounding the core and extending to the grain margin), and overgrowths (parts of grains that have grown unconformably around or infilled reentrants in partly resorbed zircons). Partly resorbed cores that are dark in cathodoluminescence (CL) images of sectioned zircon in Stevens samples, as well as a growing body of literature that documents presence of zircon antecrysts in volcanic and plutonic rocks that predate eruption or solidification by ~10^4 to a few times 10^6 yr (e.g., Brown and Fletcher, 1999; Reid, 2003; Charlier et al., 2005; Bacon and Lowenstern, 2005; Matzel et al., 2006; Miller et al., 2007; Walker et al., 2007), suggest that antecrysts are likely present in Tatoosh intrusive suite samples. At 20 Ma, roughly the age of the Tatoosh intrusive suite plutons, rigorous identification of zircon antecrysts on the basis of age requires analytical precision sufficient to resolve ages that differ by as much as ~10% to as little as ~0.05%. Accordingly, between 11 and 31 SIMS analyses of zircons from each of the six samples studied with the sensitive high-resolution ion microprobe–reverse geometry (SHRIMP-RG) were evaluated using Isoplot 3.41 (Ludwig, 2003) in order to define statistically robust crystallization ages and zircon age populations. Precision of SHRIMP-RG U-Pb data for Tatoosh intrusive suite zircons was sufficient for clear definition of solidification ages, but it limited identification of antecryst populations to those with ages ~1 m.y. greater than solidification ages of host magmas. Zircon crystallization durations, or crystal/overgrowth intervals, were sufficiently short that some nominal ages obtained on cores were younger than corresponding rims, though the two ages were indistinguishable at the ±2σ level (e.g., grain 116 in sample 203010; Table DR6 [see footnote 1]). The mean and median 2σ uncertainties of 115 Tatoosh intrusive suite zircon analyses are 0.57 and 0.56 m.y. (3.1%), respectively; the minimum is 0.25 (1.4%), and the maximum is 1.09 (5.7%).

Initial attempts to determine solidification ages using data obtained for two grain mounts during separate SHRIMP-RG sessions were compromised by instrument instability and calibration differences. Trace-element concentrations determined in these sessions have been used in the present study, but the U-Pb ages have not. Acquiring an internally consistent U-Pb data set with best possible precision required a third analysis session in which crystals from all six samples were placed in a single mount that was analyzed during a continuous 65 h period; U, Th, Hf, and REE concentrations were measured concurrently. In order to maximize precision and monitor accuracy, zircons were analyzed in a "round robin" procedure, in which single spots were analyzed from each of three samples and the R33 standard in succession before repeating the procedure for a second zircon from each, and so on; one of three samples analyzed always was 203080, which contains relatively large, U-rich zircon that is uniform in age within the resolution of the SHRIMP-RG. Subparallel trends in $^{206}Pb/^{238}U$ spot ages of R33 and 203080 with time during some parts of the analytical session suggest that not all variation in apparent ages of these zircons is random or represents true age differences but may reflect either instrument drift or position in the grain mount, or both factors (Fig. DR29 [see footnote 1]). These trends do not appear to be significant at the ±2σ level. The fact that ages for the other samples (e.g., 203010) commonly do not covary with either the R33 or 203080 ages implies that at least some intrasample age differences are real. Ireland and Williams (2003, p. 219) caution that calibrations for SIMS determination of Pb/U ratios, and therefore ages, become increasingly biased for U once its concentration exceeds ~3000 ppm. Because only six of the points on Tatoosh intrusive suite zircon that were used for geochronology have >1000 ppm U, and the maximum is 2200 ppm, we presume that the calibration is satisfactory for the entire zircon suite.

Geochronologic data for each sample are summarized in Table 7 and presented in their entirety in Table DR6 (see footnote 1). The $^{206}Pb/^{238}U$ spot ages have been corrected for initial U-Th disequilibrium using measured zircon $^{232}Th/^{238}U$ ratios, whole-rock Th and U values, and expressions given by Crowley et al. (2007, their Data Repository); although whole-rock Th/U probably is not equivalent to that of the melt that precipitated zircon, varying whole-

TABLE 6. RECONAISSANCE ISOTOPIC DATA FOR SAMPLES OF THE TATOOSH INTRUSIVE SUITE PLUTONS, MOUNT RAINIER NATIONAL PARK, WASHINGTON

Sample no.	Pluton	$^{143}Nd/^{144}Nd$	Error (2σ)	$^{87}Sr/^{86}Sr$	Error (2σ)	$^{206}Pb/^{204}Pb$	$^{207}Pb/^{204}Pb$	$^{208}Pb/^{204}Pb$	$\delta^{18}O$ (‰)
203004	Nisqually	0.512909	0.000010	0.703719	0.000009	18.9528	15.5844	38.6184	7.8
203080	Pyramid	0.512874	0.000003	0.703905	0.000009	18.9838	15.5900	38.6789	11.0
203085	Stevens	0.512898	0.000005	0.703933	0.000008	19.0073	15.5919	38.7064	0.4
93T059	Reflection	0.512897	0.000004	0.703870	0.000007	18.9520	15.5919	38.6633	7.4

rock Th/U does not change the correction substantially. This correction typically amounts to about +0.09 m.y.; quoted uncertainties in U-Th-disequilibrium–corrected ages include propagated uncertainties in zircon and whole-rock Th/U ratios (±5% and ±12%, 1σ, respectively), though this adds only about ±0.001 m.y. to the total uncertainty of any spot analysis. The solidification age of a sample is probably best represented by the TuffZirc age (Ludwig and Mundil, 2002), which is the median and its uncertainty for a group of analyses that are coherent within analytical error, and which accounts for statistical limitations on resolution of complexity in the true age-structure of a suite of analyses. We interpret ages rejected by TuffZirc on the young side of a distribution to have been affected by Pb loss and those rejected on the old side to be antecrysts. Weighted mean ages for the same groups of analyses are similar to the TuffZirc ages, although they typically have somewhat lower uncertainties (at 95% confidence). Reported ages of populations (unmix ages), 2σ uncertainties, and fractions of the total sample were calculated by Isoplot using the mixture-modeling algorithm of Sambridge and Compston (1994) for deconvolution of a population of dates that contains multiple age components. Results are consistent with those obtained by TuffZirc, and they suggest that the youngest ages for sample 203004 may have been affected by Pb loss and that zircons with ca. 20 Ma ages in samples 203010 and 203085 are antecrystic.

The sample of Nisqually pluton from Paradise Valley (203004), the geochronologic sample innermost within the nested units of the Tatoosh intrusive suite (Fig. 1), yields the youngest solidification age, 17.29 +0.37/–0.24 Ma (Fig. 7A). It is unclear whether the three or four analyses that yield younger ages have been affected by Pb loss or are, in fact, significantly younger than the main population; fewer analyses were obtained for this sample than for others. The Nisqually pluton sample (203000) from the Nisqually River canyon at Christine Falls yielded a solidification age of 17.70 +0.30/–0.16 Ma (Fig. 7B). Results for these two samples are indistinguishable from the 17.5 ± 0.1 Ma TIMS U-Pb concordia-intercept age reported by Mattinson (1977), which, were it corrected for initial U-Th disequilibrium, probably would be 17.6 ± 0.1 Ma.

Reflection phase (93T059) from the Pinnacle Peak trail has a solidification age of 18.38+0.45/–0.28 Ma. Although the relative probability curve is bimodal (Fig. 7C) and mixture modeling yields 18.10 ± 0.23 and 18.83 ± 0.24 Ma (Table 7), analysis with TuffZirc suggests that division into two populations is not statistically robust. Consistent with this conclusion, there is a lack of any simple correlation between measured zircon age and elemental concentrations or ratios. U-Pb results for this sample exemplify the limitations in extracting meaningful ages from subpopulations that rock texture suggests are likely present but are masked by analytical uncertainties.

Zircon ages for the Pyramid phase (203080) have a highly symmetrical probability distribution (Fig. 7D). All 31 zircon analyses, including the three of rims, define a TuffZirc solidification age of 18.58 +0.20/–0.15 Ma; this is despite the fact that zircon trace-element concentrations span considerable ranges in this sample. Analytically indistinguishable solidification ages for the Reflection and Pyramid samples, along with their similar zircon trace-element abundances and ratios, imply that these texturally distinct rock units share a close genetic relationship that is consistent with field relations.

Two samples (203010 and 203085) of the Stevens pluton, from localities separated by 3 km, yielded relatively complex zircon populations that have similar varieties of internal zonation visible in CL, comparable trace-element abundances, and virtually identical solidification ages of 19.15 +0.15/–0.12 Ma and 19.20 + 0.31/–0.26 Ma. Moreover, analyses that reflect the older, subsidiary mode in relative probability diagrams and that were rejected by TuffZirc (Figs. 7E and 7F) give indistinguishable weighted mean values of 20.18 ± 0.26 and 20.07 ± 0.18 Ma, which are corroborated by mixture modeling (Table DR6 [see footnote 1]). These ca. 20 Ma zircons are interpreted as antecrysts. An overgrowth on one of them (115.1 in sample 203085) has a relatively precise age of 20.0 ± 0.3 Ma that implies that overgrowths are of more than one age. One zircon from sample 203010 gave a $^{206}Pb/^{238}U$ age of 89.0 ± 1.4 Ma (2σ) for its core and 18.0 ± 0.8 Ma for its outer part; this is the only zircon xenocryst identified in any of the six Tatoosh intrusive suite samples. The greater variety of resolvable zircon ages that include antecrysts and a Cretaceous xenocryst, diversity of trace-element concentrations and ratios, and abundance of partly resorbed CL-dark cores in the Stevens pluton relative to the other Tatoosh intrusive suite samples are consistent with these being the earliest intruded, compositionally most differentiated magmas in which recycled zircon was least likely to completely dissolve before solidification.

U, Th, Hf, AND REE IN ZIRCON

Concentrations of U, Th, Hf, and REE (Table DR7 [see footnote 1]) vary substantially among zircons in a single igneous rock. Core-rim differences and patterns of relative elemental concentrations help to define zircon populations and affinities between samples. The extent of differentiation of melts from which zircons grew and the influence of fractionating assemblages can be inferred from trace- and minor-element concentrations in zircon and zircon-melt partition coefficients. Zircon provenance thus inferred can indicate mixed populations that result from magma mixing or recycling of antecrysts. Sector zoning and fine-scale oscillatory zoning visible in CL images serve as reminders that zircon-melt partition coefficients or kinetic factors may vary between growth surfaces and that the footprint of the ion probe beam averages concentrations across micrometer-scale changes in concentration that may contain values more

TABLE 7. SUMMARY OF SENSITIVE HIGH-RESOLUTION ION MICROPROBE–REVERSE GEOMETRY (SHRIMP-RG) $^{206}Pb/^{238}U$ GEOCHRONOLOGIC DATA FOR TATOOSH INTRUSIVE SUITE PLUTONS, MOUNT RAINIER NATIONAL PARK, WASHINGTON

Sample	Unit	TuffZirc age (Ma)	Weighted mean age (Ma)	*n*	MSWD	Probability	Unmix ages (Ma)	Fraction
203004	Nisqually	17.29 +0.37/–0.24	17.36 ±0.31	8/11	2.2	0.033	16.62 ±0.66	0.37
							17.46 ±0.23	0.63
203000	Nisqually	17.70 +0.30/–0.16	17.96 ±0.18	15/17	1.6	0.079	–	–
93T059	Reflection	18.38 +0.45/–0.28	18.49 ±0.23	13/16	1.9	0.026	18.10 ±0.23	0.48
							18.83 ±0.24	0.52
203080	Pyramid	18.58 +0.20/–0.15	18.61 ±0.11	31/31	1.5	0.049	–	–
203010	Stevens	19.15 +0.15/–0.12	19.12 ±0.17	16/20	1.6	0.072	19.11 ±0.13	0.86
							20.18 ±0.26	0.14
203085	Stevens	19.20 +0.31/–0.26	19.25 ±0.16	16/20	1.7	0.050	19.22 ±0.12	0.71
							20.07 ±0.18	0.29

Note: TuffZirc age calculated by Isoplot 3.41 is the age and uncertainty of the median of a coherent group of analyses (Ludwig and Mundil, 2002). Weighted mean age reports uncertainties at 95% confidence; *n*—number of analyses used for TuffZirc and weighted mean ages/total number of analyses; MSWD—mean square of weighted deviates; probability—probability of fit. Unmix ages and fractions were calculated by Isoplot 3.41 using the algorithm of Sambridge and Compston (1994); uncertainties are ±2σ.

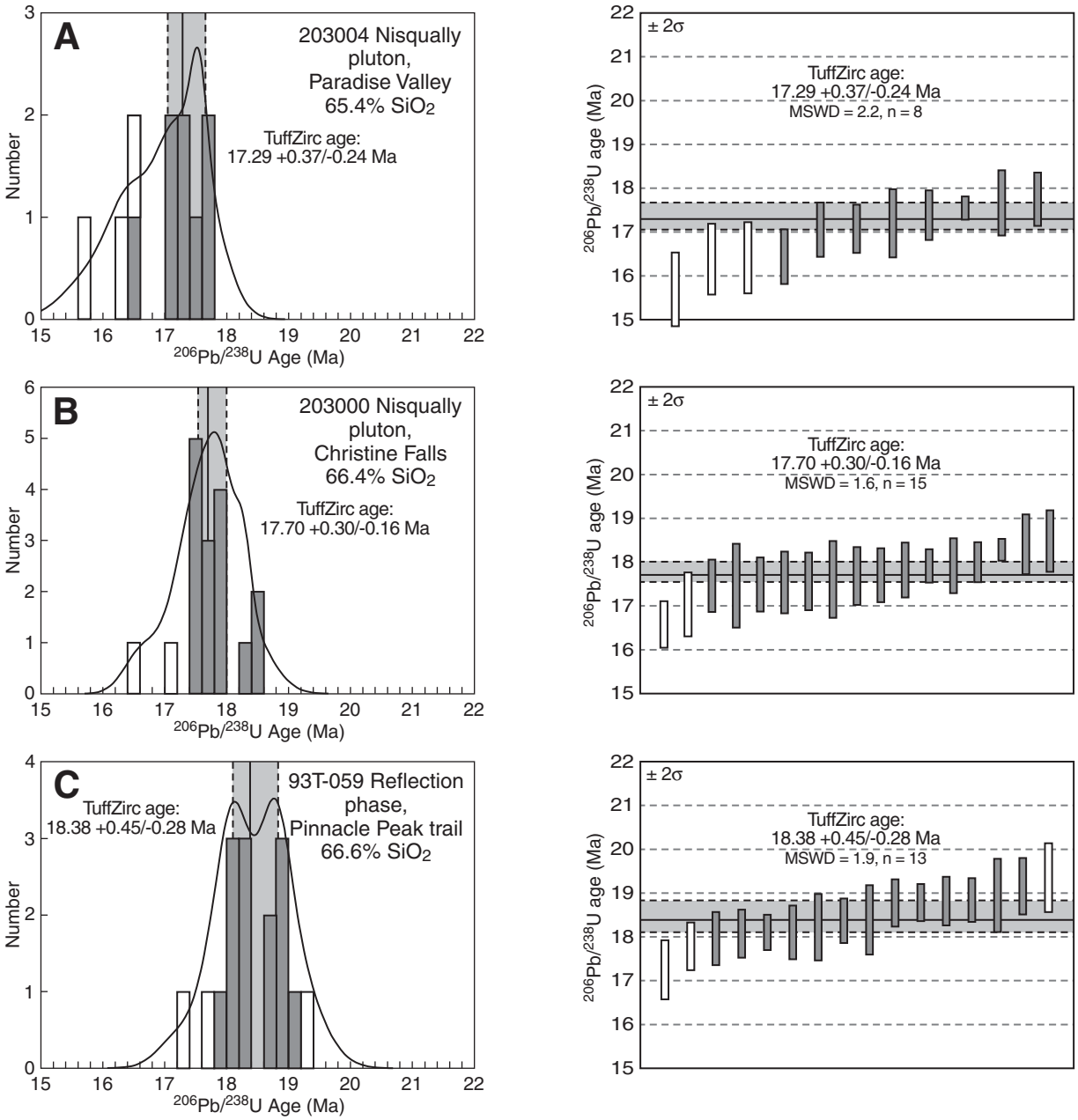

Figure 7 (*continued on following page*). Sensitive high-resolution ion microprobe–reverse geometry (SHRIMP-RG) $^{206}Pb/^{238}U$ ages for zircon, corrected for initial U-Th disequilibrium, from six Tatoosh intrusive suite samples. For each sample, left panel is an age histogram of spot analyses along with a relative probability distribution (curve) and TuffZirc age and associated uncertainty (vertical solid and dashed lines, respectively, with interval shaded). Ages represented by shaded histogram bars were used in TuffZirc and weighted mean age calculations. Ages of antecrysts in E and F are weighted means with 95% confidence limits of those populations (white bars at right). Right panels show ages and ±2σ uncertainties on individual analyses for zircons from each sample, along with TuffZirc and antecryst ages and uncertainties as in left panels. MSWD—mean square of weighted deviates. (A) Nisqually pluton, sample 203004. (B) Nisqually pluton, sample 203000. (C) Reflection phase, sample 93T059. (D) Pyramid phase, sample 203080. (E) Stevens pluton, sample 203010. (F) Stevens pluton, sample 203085.

extreme than any revealed by SIMS (other than nanoSIMS). Analyses referred to here as "rim" in reality are from the outermost ~40 µm of sectioned crystals.

Zircon compositional variation in the six Tatoosh intrusive suite samples analyzed for U-Pb geochronology ranges from modest in the Pyramid phase to substantial in the Stevens pluton. Extreme values and wide ranges in trace-element concentrations and some element ratios indicate that many analyzed zircons grew in highly fractionated residual liquids that had experienced significant crystallization. Concentrations of Th and U in Tatoosh intrusive suite zircons vary across two orders of magnitude (Fig. 8). Zircon interiors in all six samples tend to have higher Th and U contents than rims. With few exceptions, Th/U ratios are 0.3–2. Although zircon preferentially incorporates U relative to Th (Blundy and Wood, 2003), cores within a population commonly have higher Th/U ratios than rims. Precipitation of thorite, or possibly allanite, during zircon rim growth may be responsible for lowering melt Th/U. Late overgrowths that fill reentrants in zircon from the Stevens pluton, and in three zircons from the Nisqually pluton, have high U contents and Th/U ratios of 0.05–0.3. Greater range and scatter in Th and U values for zircons from the Stevens pluton compared to those of other Tatoosh intrusive suite samples, and rim values clustered at relatively low Th, U, and Th/U values, reflect the presence of at least two major zircon populations, one of which commonly occurs as partly resorbed, CL-dark cores that may make up most of a cross section of a given crystal. The low-U, Th/U ≈ 0.5 rims on all types of cores reflect growth in Stevens granitic melt, whereas the partly resorbed cores, the mean ^{238}U-^{206}Pb ages of which are irresolv-

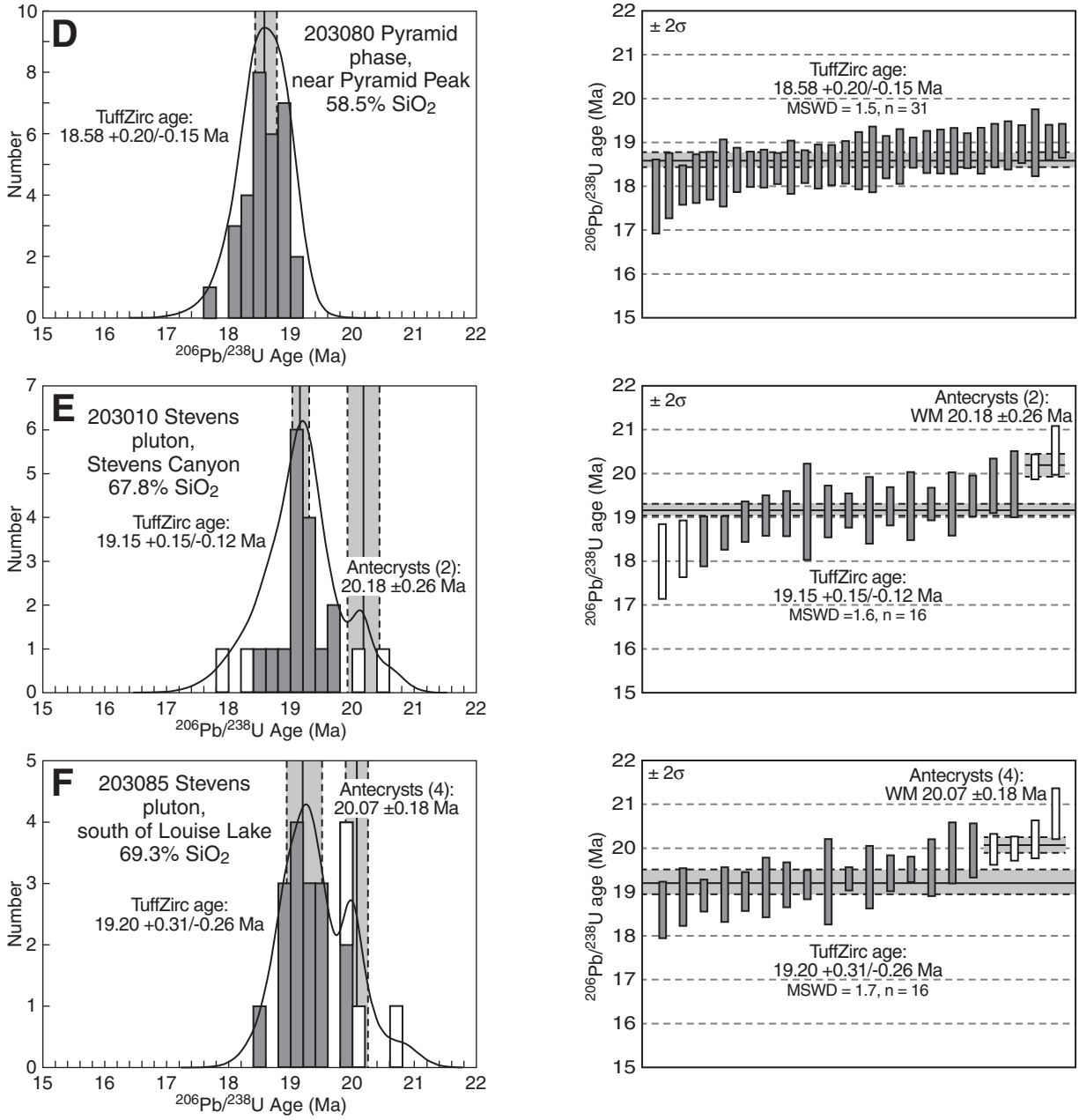

Figure 7 (*continued*).

able from those of rims, and the few crystals with ages of ca. 20 Ma evidently are antecrysts. The sole pre-Miocene core, 89.0 ± 1.4 Ma, has an 18.0 ± 0.8 Ma rim that falls within the range of core U and Th concentrations (Fig. 8E).

The utility of Hf concentration in zircon as an index of relative magma fractionation extent was pointed out by Claiborne et al. (2006), who demonstrated that Hf concentrations generally increase with the degree of melt fractionation. Hafnium in Tatoosh intrusive suite zircon populations does not covary simply with U or Th but is a useful melt differentiation index. Low-U zircon rims from Stevens samples typically have higher Hf than cores of the same crystals, which

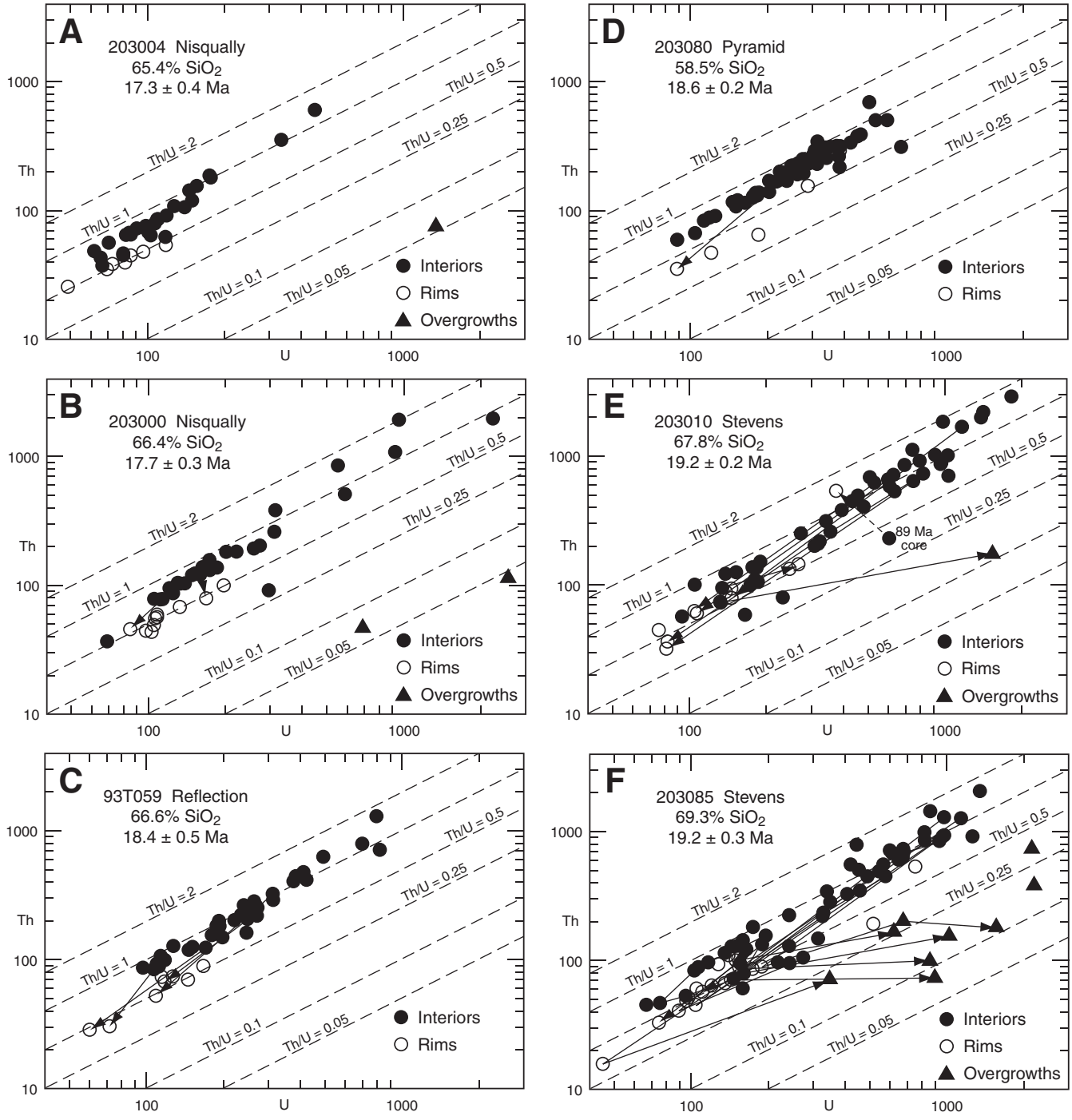

Figure 8. Concentrations of Th and U (ppm) measured by sensitive high-resolution ion microprobe–reverse geometry (SHRIMP-RG) in zircon from six Tatoosh intrusive suite samples. Lines of constant Th/U ratio (dashed) are shown for reference. Arrows connect points for interior, rim, and overgrowth parts of a single crystal. (A) Nisqually pluton, sample 203004. (B) Nisqually pluton, sample 203000. (C) Reflection phase, sample 93T059. (D) Pyramid phase, sample 203080. (E) Stevens pluton, sample 203010. (F) Stevens pluton, sample 203085.

suggests that partly resorbed cores were overgrown by zircon precipitated from relatively evolved liquid. Reliability of Hf as a differentiation index of zircon parent melts for individual zircons is evident in plots of Eu/Eu* versus Hf concentration (Fig. 9). Two parallel arrays (Figs. 9A–9D), in which Eu/Eu* decreases systematically as Hf increases and rims tend to have higher Hf than most cores, are consistent with growth of higher Hf, lower Eu/Eu* zircon from more evolved melts. The separate arrays suggest that the two Nisqually samples are from one intrusive system and the Pyramid and Reflection are samples from another. Eu/Eu* values indicate that zircon of both arrays grew from evolved melts that had experienced substantial feldspar crystallization and that those for the Reflection and Pyramid phases were either more evolved or, possibly, less oxidized than those in the Nisqually pluton. Zircon Eu/Eu* and Hf values in the two Stevens pluton samples have significantly greater ranges (Figs. 9E and 9F), consisting of a high Eu/Eu* field and one rather similar to that for the Reflection and Pyramid samples. Most partly resorbed zircon cores in the Stevens samples grew in melts that were less evolved or more oxidized than did rims and other zircons. Rims of both high and low Eu/Eu* core populations retain Eu/Eu* values comparable to those of their cores but have higher Hf contents. High-Hf overgrowths on the Stevens and one Nisqually zircon, which have high-U and low-Th/U values, grew from late-stage highly differentiated melts or fluids that consequently had substantially diverse trace-element concentrations, but they typically are zoned toward low Eu/Eu* ratios. The ^{238}U-^{206}Pb age of an overgrowth on a Nisqually zircon is indistinguishable from the TuffZirc age of zircon in that sample, while the 20.0 ± 0.3 Ma age of an overgrowth on a Stevens zircon appears to be significantly older than most zircon analyzed in that sample. Scatter in Eu/Eu* of overgrowths, and the one overgrowth age from the Stevens sample, suggests that overgrowths may represent a number of separate, incremental solidification events. Eu/Eu* variations may also reflect a diversity of near-solidus melt compositions due to loss of interconnectivity and failure to maintain melt homogeneity.

Chondrite-normalized REE diagrams for Tatoosh intrusive suite zircons (Fig. 10) have a familiar convex-up shape with positive Ce and negative Eu anomalies (Belousova et al., 2002; Hoskin and Schaltegger, 2003): La_N = 0.03–6 (10 values >6 may reflect inclusions of other phases; 31 of 268 values are >1), Yb_N = 380–33,900, Ce/Ce* = 0.7–505 (only one value is <1 and 19 are <10), and Eu/Eu* = 0.06–1.25 (only 3 values are ≥1). Overall, slopes of typical REE patterns subtly increase in the order Reflection < Pyramid ≤ Nisqually < Stevens (though some Stevens REE slopes are among the lowest), which is principally due to HREE concentration variation. The greatest ranges in zircon REE concentrations are in the Stevens samples, in which partly resorbed cores have the highest REE abundances and rims have the lowest. In fact, analyzed rims mainly have lower REE concentrations and steeper patterns than cores in the same sample. Stevens zircon overgrowth REE patterns have LREE and MREE concentrations similar to those of rims, but HREE values are midrange, so that overgrowth patterns are the steepest (Figs. 10E and 10F). The sole analyzed Nisqually overgrowth also has low REE concentrations and a pattern with a steep slope (Figs. 10A and 10F).

Fractionation of plagioclase + pyroxene and (or) amphibole + Fe-Ti oxide + apatite + zircon in typical modal proportions should produce successive liquids in which LREE concentrations increase more rapidly than do HREE, i.e., REE patterns become more steeply negatively sloping with differentiation. The fact that Tatoosh intrusive suite zircon REE concentrations do not show a simple progression with rock composition or age is consistent with existence of at least three major intrusive systems. Subparallel REE patterns among zircons from individual samples of the Nisqually pluton and Reflection and Pyramid phases suggest that those zircons grew in melts that could have differentiated from a specific consanguineous parent magma for each sample (e.g., within separated domains in crystallizing mush). Marginally more positively sloping patterns for rims, and lower REE concentrations, may result from coprecipitation of LREE-enriched allanite. As is characteristic of other trace elements, the REE in zircons from Stevens samples vary in ways that imply more than one parental magma. Finally, Stevens zircon overgrowths, and the one Nisqually example, have REE patterns that indicate crystallization from evolved melts or fluids that were either relatively HREE rich or in fluids where crystallization occurred under conditions at which zircon-melt partition coefficients more strongly favored HREE than is typical of commonly sampled magmatic environments.

ASSEMBLY AND SOLIDIFICATION OF THE TATOOSH INTRUSIVE SUITE

The Tatoosh intrusive suite plutons represent repeated emplacement and solidification of magma to form a nested plutonic complex. Solidification of the three Tatoosh intrusive suite magma pulses (Stevens, Reflection-Pyramid, and Nisqually) was separated by ~0.7–1.0 m.y. intervals. U-Pb zircon ages for pairs of samples from the Stevens and Nisqually plutons (members of each pair collected ~3 km apart) are each statistically indistinguishable. Similarly, one sample each from the consanguineous Reflection and Pyramid phases (samples collected ~6 km apart) also yield statistically indistinguishable ages. The lack of age differences resolvable by SIMS within the relatively small Tatoosh intrusive suite plutons contrasts with observations of Coleman et al. (2004) of multiple zircon ages, spanning millions of years, for individual Tuolumne intrusive suite constituent plutons. Consequently, our age data for the Tatoosh intrusive suite do not support the incremental assembly scenario described by Coleman et al. (2004) and Glazner et al. (2004). However, dated zircon antecrysts in Stevens pluton samples (and possibly in samples of other Tatoosh intrusive suite plutons) imply that generation, emplacement, and solidification of the magma that formed each pluton were not necessarily single-stage processes.

Although the precision of zircon geochronologic data precludes rigorous identification of zircon antecrysts from older Tatoosh intrusive suite plutons in its younger plutons, zircon trace-element characteristics are sufficiently distinct to allow identification of exotic crystals. Preservation of an 89 Ma zircon xenocryst in a Stevens sample suggests antecryst survivability in that pluton. In fact, the Nisqually, Pyramid, and Reflection samples contain only zircon crystals with compositions similar to other zircons contained in their respective plutons. Consequently, either Nisqually and Reflection-Pyramid plutons were zircon undersaturated at the time of emplacement and destroyed earlier-formed zircon crystals, or they interacted minimally with earlier-emplaced Tatoosh intrusive suite plutons. Zircon's refractory character inhibits its ready dissolution (Watson, 1996). Despite their nested emplacement, Tatoosh intrusive suite plutons apparently inherited limited input from earlier-emplaced intrusions.

We infer that each of the three main magma pulses consisted of a variably crystal-rich magma batch that rose buoyantly some distance from its original accumulation site. Each pulse probably represents the amalgamated remains of long-lived systems, possibly with lifetimes of hundreds of thousands of years, that likely fed superjacent volcanoes. The compositional trend within the Tatoosh intrusive suite to less-evolved bulk compositions possibly reflects progressive depletion of the most readily fusible material from the underlying crustal section or, alternatively, secular warming of the intrusive environment. Emplacement of Tatoosh intrusive suite plutons at a depth of 1–2 km is indicated

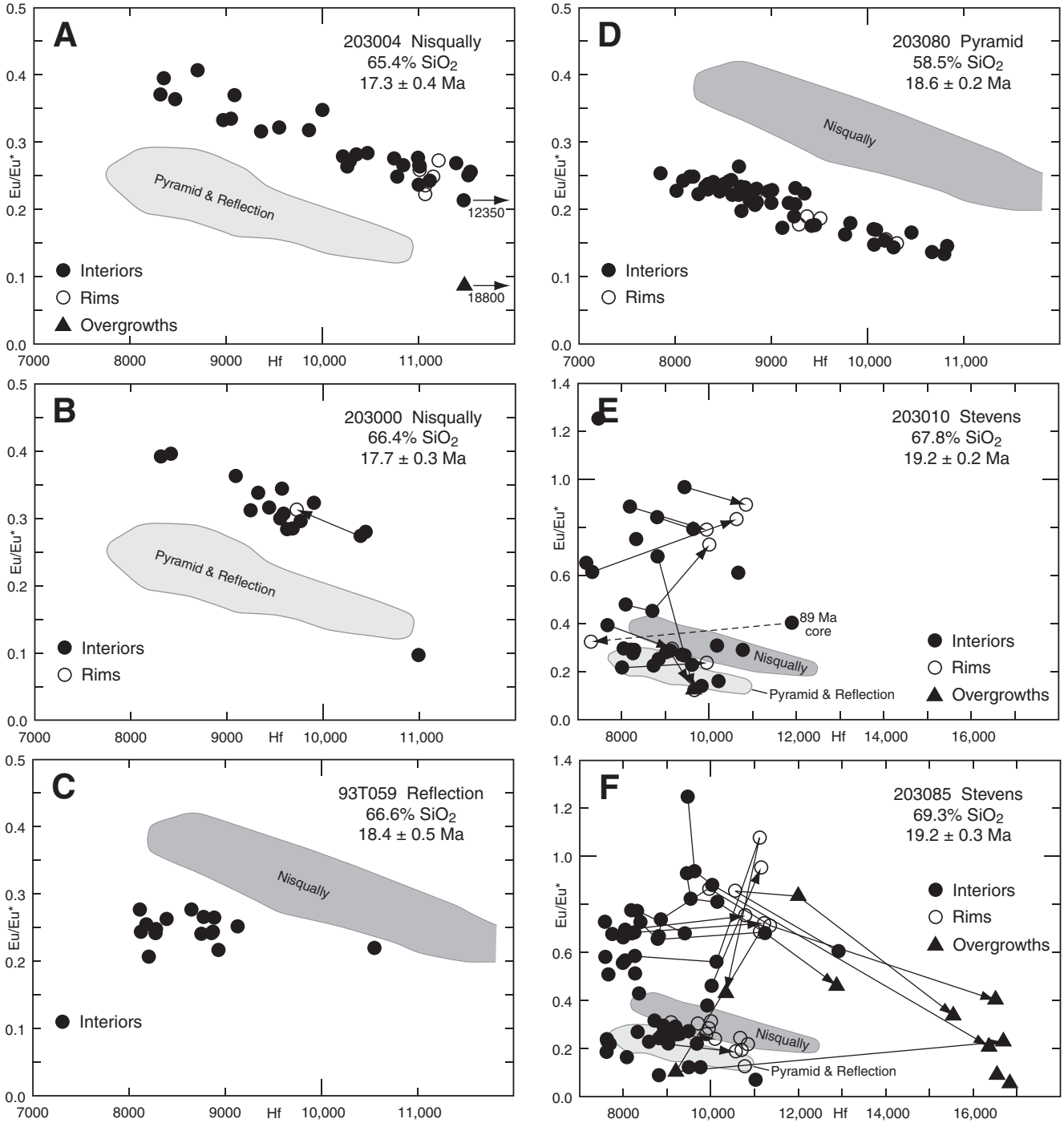

Figure 9. Concentration of Hf (ppm) and ratio Eu/Eu* measured by sensitive high-resolution ion microprobe–reverse geometry (SHRIMP-RG) in zircon from six Tatoosh intrusive suite samples. Arrows connect points for interior, rim, and overgrowth parts of a single crystal. For comparison, shaded fields enclose data for units other than plotted data. Points in E and F, with Eu/Eu* ≥ 0.5, may over-represent the true proportion of high Eu/Eu* zircon in separates. (A) Nisqually pluton, sample 203004. (B) Nisqually pluton, sample 203000. (C) Reflection phase, sample 93T059. (D) Pyramid phase, sample 203080. (E) Stevens pluton, sample 203010. (F) Stevens pluton, sample 203085.

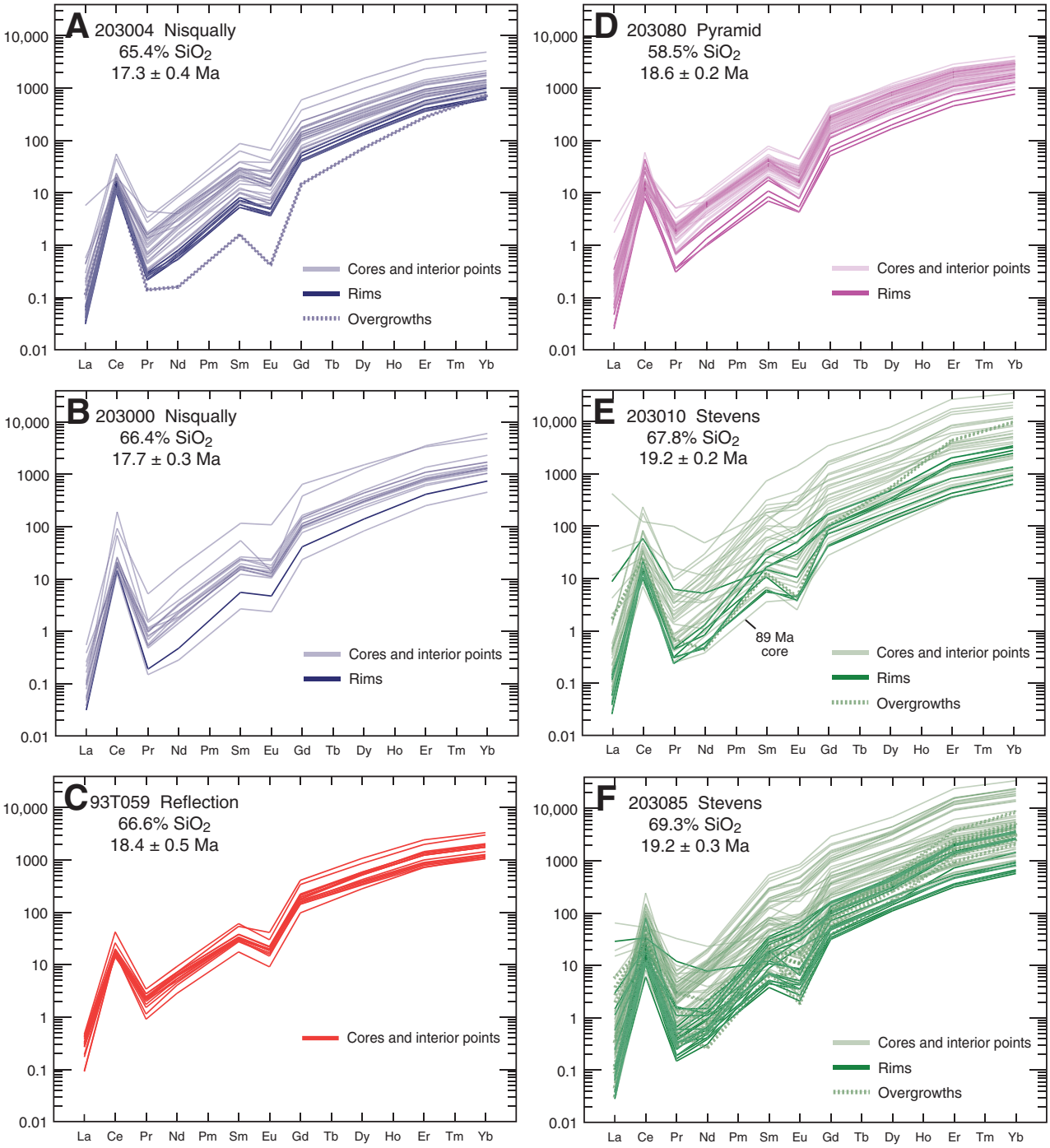

Figure 10. Chondrite-normalized concentrations of rare earth elements (REEs) in zircon from six Tatoosh intrusive suite samples. Concentrations were measured by sensitive high-resolution ion microprobe–reverse geometry (SHRIMP-RG) for La, Ce, Nd, Sm, Eu, Gd, Dy, Er, and Yb. Chondrite concentrations are from Anders and Grevesse (1989), as modified by Korotev (1996). (A) Nisqually pluton, sample 203004. (B) Nisqually pluton, sample 203000. (C) Reflection phase, sample 93T059. (D) Pyramid phase, sample 203080. (E) Stevens pluton, sample 203010. (F) Stevens pluton, sample 203085.

by stratigraphic reconstructions of roof rock thickness and is consistent with low host-rock metamorphic grade, granophyric mesostasis content, and lithologic characteristics of the Mazama Ridge breccia.

Within-pluton compositional variation implies final fractionation processes dominated by differential separation (unmixing) of crystals from residual liquid via compaction (Bachmann and Bergantz, 2004) or gas-driven filter pressing (Sisson and Bacon, 1999); some extracted residual liquid may have been reinjected to form aplite dikes. Some crystals in Tatoosh intrusive suite samples may represent "crystal cargo" recycled from plutonic rock or crystal mush (Davidson et al., 2007). As is increasingly well documented (e.g., Andrews et al., 2008), the products of arc magmatism preserve evidence of recharge, assimilation, and hybridization. Within the Tatoosh intrusive suite, the presence of enclaves and zoning profiles in plagioclase (Item DR4, Table DR4, and Fig. DR7 [see footnote 1]), for instance, indicate that these processes contributed to Tatoosh intrusive suite petrogenesis. Tatoosh intrusive suite enclaves and mafic dikes may represent relatively unfractionated magmas (Fig. 4, 93T159) that approximate compositions (Table 4) of recharge and (or) parental magmas derived from reservoirs associated with subduction processes. Processes ultimately responsible for compositional evolution within Tatoosh intrusive suite plutons were likely not entirely restricted to melt extraction but probably also involved various crystal-liquid reactions and multiple-source magma mixing.

The timing and processes responsible for development of crustal magma chambers have been much studied and debated (e.g., Glazner et al., 2004; Coleman et al., 2004; Lipman, 2007; Walker et al., 2007), particularly whether these accumulate and substantially solidify incrementally during as much as millions of years or form large, long-lived magma chambers capable of convective homogenization and incremental and (or) episodic solidification. By comparison, Hirt (2007) suggested a genesis for large plutons in the southern Sierra Nevada batholith involving a combination of these processes and reflecting the thermal status of the upper crust. Importantly, individual plutons throughout the world are characterized by distinctive geochemical and mineralogical compositions, textures, grain size, and zonation, and generally lack internal contacts (e.g., Bateman, 1992), and abundant evidence exists to demonstrate that exceptionally large volumes (pluton to batholith scale) of eruptible (<50% crystals) magma must have resided in upper-crustal reservoirs prior to eruption (Lipman, 2007). The pluton emplacement hypothesis of Glazner et al. (2004) and Coleman et al. (2004) suggests that plutons consist of incrementally assembled magma batches and that each magma increment substantially solidifies before emplacement of the next. Such a process largely precludes pluton homogenization/zonation. In contrast, the apparent lack of internal contacts, compositional and textural homogeneity, and evidence of variable interstitial melt extraction preserved within the Tatoosh intrusive suite indicate development of a single magma body at the level of emplacement. Accordingly, each of the Tatoosh intrusive suite plutons appears to have intruded to the present level of exposure, coalesced as a single magma body, and solidified slowly enough that convective homogenization minimized any internal variation beyond that produced by variable interstitial melt extraction.

HYDROTHERMAL ALTERATION OF THE TATOOSH INTRUSIVE SUITE

Most rocks of the Tatoosh intrusive suite have been affected by various types of pervasive but generally weak hydrothermal alteration. Among the Tatoosh intrusive suite plutons, the Stevens pluton includes the largest area of altered rock and is also the most intensely altered, perhaps because it is the oldest pluton and was subjected to superimposed alteration related to the younger intrusions. Alternatively, because the Stevens pluton is the only Tatoosh intrusive suite pluton with significant exposed contacts with older rocks, this pluton may be more altered because it could interact with the country rocks and hydrothermal fluids that flowed through those rocks. With the exception of the Stevens pluton and the Pyramid phase, magmatic sulfide minerals are absent, which suggests that magmas represented by the Tatoosh intrusive suite plutons contained relatively low sulfur abundances and (or) lost most contained sulfur during the cooling and shallow degassing processes indicated by granophyric textures. Sulfide minerals also are uncommon in altered rocks. Most Tatoosh intrusive suite samples are incompletely altered, and alteration features and minerals are transitional between alteration types in many samples. Alteration intensity is greatest in the Stevens pluton and Pyramid phase (Fig. 11A) and least in the Nisqually pluton, except for small, more intensely altered areas in its southeast part. Megascopic veins are widely distributed but nowhere are they sufficiently abundant to form stockwork or sheeted vein systems (Fig. 11B). Although incomplete exposure precludes a thorough evaluation of vein density, veins seem to be most abundant in the Paradise Valley and Mazama Ridge areas. Veins in older Tatoosh intrusive suite plutons are truncated at contacts with younger plutons. Most veins are ≤1 mm, and few are >1 cm wide. Bleached selvages around many actinolite veins are as much as several centimeters wide.

Dominant alteration types are deuteric, propylitic, and biotitic (Fig. 11C); the breccia pipe on Mazama Ridge (Wright, 1961) was affected by local sodic-calcic alteration. Crosscutting relations near the roof of the Stevens pluton in the Tatoosh Range indicate that propylitic alteration predates biotitic alteration, whereas early biotite veins are cut by later actinolite veins at the Nisqually mines, a largely concealed pair of adits in the Reflection phase. Elsewhere, paragenetic vein and alteration relations are indeterminate.

Weak deuteric alteration is the most common alteration type (Fig. 11C). It consists of incipient plagioclase replacement by sericite and (or) other microcrystalline clay minerals, partial biotite replacement by chlorite and hornblende by actinolite and (or) biotite, and perthitic exsolution of alkali feldspar. With increasing alteration intensity, deuteric alteration grades into propylitic alteration. In propylitized rocks, many plagioclase crystals are antiperthitic, altered to more sodic compositions along irregular microfractures, and partly replaced by epidote, sericite, and (or) calcite. Fibrous actinolite replaces hornblende and pyroxene crystals, and chlorite, titanite or rutile, and Fe-oxide minerals replace biotite. Alkali feldspar crystals are distinctly turbid and coarsely perthitic but are not replaced by clay minerals or sodic plagioclase. Tourmaline is locally disseminated in altered groundmass. Narrow (generally <1–2 mm), widely distributed actinolite veins with pronounced bleached selvages as much as 2–3 cm wide are a prominent manifestation of propylitic alteration (Fig. 11B). Some actinolite veins contain magnetite, chlorite, epidote, quartz, tourmaline, and (or) pyrite. In some places, vein selvages consist of an inner zone of sodic plagioclase + sericite and an outer zone of sericite and chlorite with relict alkali feldspar. Dominant mineral assemblages in other vein types related to propylitic alteration include quartz + chlorite, chlorite, and tourmaline. Propylitic alteration is most strongly developed along the outer margins and near the roof of the Stevens pluton in the Tatoosh Range and in the Pyramid phase.

Biotitic alteration is widespread in the Tatoosh intrusive suite, but it most commonly affects the Stevens pluton (Fig. 11C). Biotitic alteration is characterized by fine-grained, shreddy aggregates of pale-brown biotite that replace hornblende and (or) pyroxene phenocrysts and fill microveins. In many places, magnetite and (or) ilmenite are intergrown with hydrothermal biotite. Most plagioclase crystals

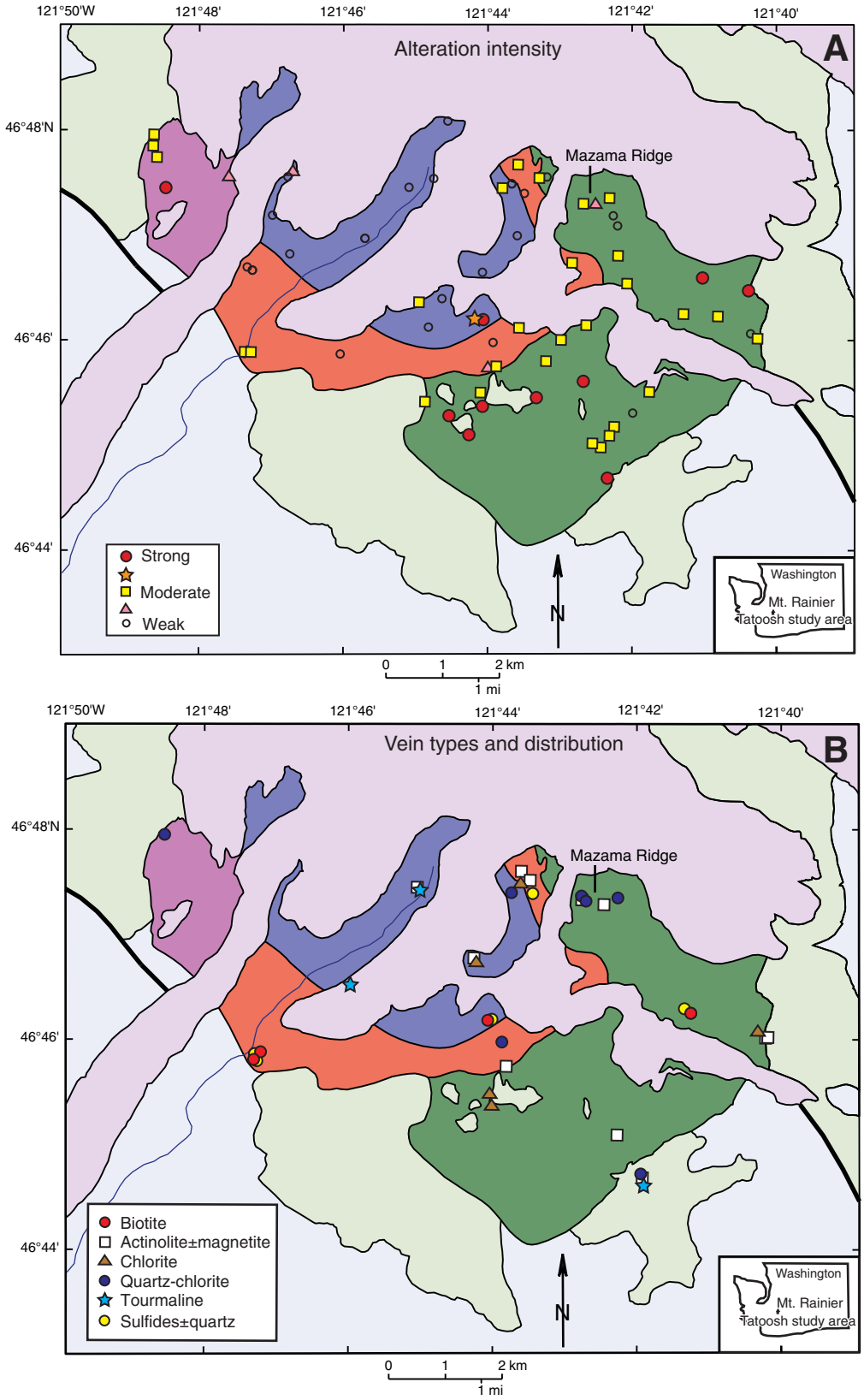

Figure 11 (*continued on following page*). Hydrothermal alteration affecting rocks of the Tatoosh intrusive suite. (A) Alteration intensity. (B) Vein distribution and type. (C) Alteration type. (D) Fluid inclusion abundance and types: type 1—liquid rich; type 2—vapor rich; type 3—high salinity.

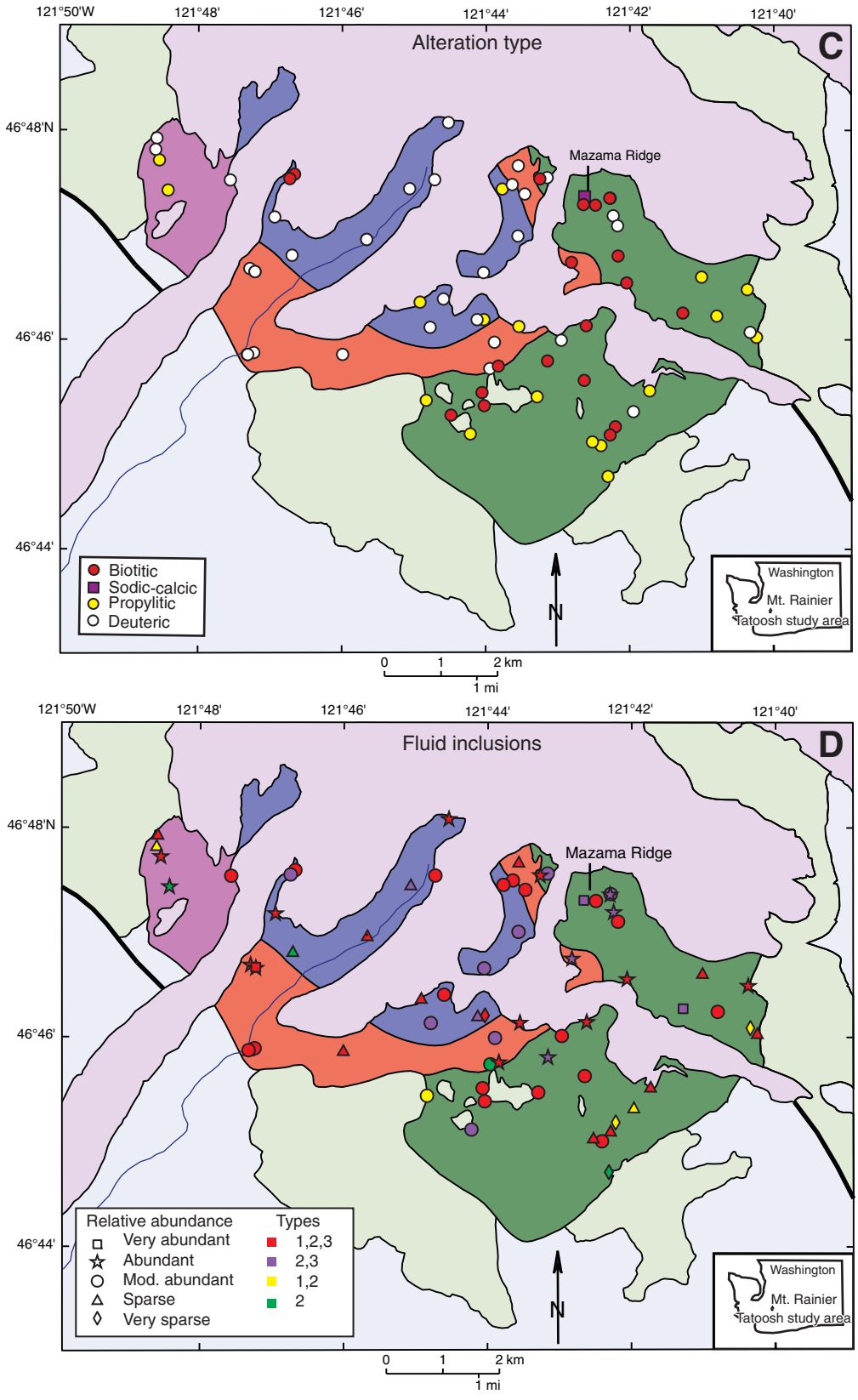

Figure 11 (*continued*).

are partly replaced by sericite, but in the most intensely biotite-altered rock, they also are locally replaced by hydrothermal biotite. Most alkali feldspar crystals are turbid and perthitic. Many areas affected by biotitic alteration are cut by sparse biotite ± quartz and sulfide veins, notably at the Nisqually mines near the southwest margin of the Reflection phase (Fig. 11B).

Sodic-calcic alteration is well developed (Fig. 11C) in the breccia pipe near the roof of the Stevens pluton on Mazama Ridge (Wright, 1961). The breccia consists of angular blocks of fine-grained granodiorite and leucocratic granite in a coarse-grained matrix of fibrous actinolite, magnetite, and apatite with small pods and zones of coarse bladed sodic scapolite, titanite, epidote, diopside, quartz, and pyrite intergrown with actinolite and magnetite. Scapolite-magnetite veins locally cut actinolite-magnetite breccia matrix. Rock fragments in the breccia are partly replaced by magnetite, actinolite, diopside, and lesser scapolite.

The small volume and low intensity of hydrothermal alteration in Tatoosh intrusive suite intrusive rocks are in accord with apparently weakly developed hydrothermal systems. Specifically, (1) alteration intensity is not well correlated with fluid inclusion abundances or types (Figs. 11A and 11D); (2) most samples with low fluid inclusion abundances are affected by deuteric or propylitic alteration (Figs. 11D and 11C); and (3) most samples that lack high-salinity inclusions are affected by deuteric or propylitic alteration near Stevens pluton margins or within the Pyramid phase.

Low fracture permeability and low water-rock ratios appear to have prevented Tatoosh intrusive suite rocks from becoming strongly altered. Regionally developed, low grade metamorphism (Fiske et al., 1963) reduced wall-rock permeability, which further inhibited development of a large convecting (meteoric) hydrothermal system. The present-day low permeability of these rocks is readily apparent at the base of the Quaternary Mount Rainier edifice, where numerous springs emanate along the interface between highly permeable Quaternary volcanic rocks and relatively impermeable Tertiary basement rocks. Fracture and vein scarcity may indicate that the Tatoosh intrusive suite magmas degassed passively during ascent and emplacement, and only released minor amounts of a fluid phase relatively late during solidification. Relatively minor (compared to other, more intensely mineralized plutonic rocks) groundmass volumes and the lack of well-developed porphyry textures in most Tatoosh intrusive suite rocks are additional manifestations of passive degassing and subsequent late H_2O-rich vapor exsolution during solidification that promoted development of weak hydrothermal convection cells responsible for Tatoosh intrusive suite rock alteration. Granophyric mesostasis likely represents rapid fluid-phase exsolution and vapor loss, possibly associated with final emplacement and (or) eruption-induced pressure-quenching events that accompanied final solidification.

CONCLUSIONS

Three moderate-size plutons on the south flank of Mount Rainier constitute the Miocene Tatoosh intrusive suite, a manifestation of ancestral Tertiary Cascades arc magmatism. The Tatoosh intrusive suite represents three separate igneous systems at the level of emplacement; this is apparent from ion microprobe U-Pb geochronologic data and observations that younger plutons intrude older, previously solidified plutons. Enclaves and fine-grained, relatively mafic rock emplaced adjacent to country rock contacts on Mazama Ridge and near the east edge and roof of the Stevens pluton have compositions that were potentially parental to those of the Tatoosh intrusive suite plutons and represent quenched, relatively less-differentiated magma, possibly derived from a deeper reservoir. Each of the three magma pulses likely represents the amalgamated intrusive products of a magmatic episode that probably was associated with intermediate to silicic volcanism. The secular trend toward less-differentiated bulk compositions may reflect increasing depletion in fusible crustal material deeper in the arc or warming of the intrusive environment.

The plutons of the Tatoosh intrusive suite were emplaced in pulses where solidification was separated by ~0.7–1.0 m.y.: Stevens pluton ca. 19.2 Ma, Reflection and Pyramid phases ca. 18.5 Ma, and Nisqually pluton ca. 17.5 Ma. Zircon antecrysts in the Stevens, the most differentiated of the plutons, record an earlier, ca. 20 Ma crystallization episode. Individual ion microprobe U-Pb zircon ages are not sufficiently precise in this age range to definitively resolve other zircon age subpopulations within Tatoosh intrusive suite plutons. Similar crystallization ages for the Reflection and Pyramid phases, similar zircon trace-element abundances, and essentially contiguous spatial distribution support their consanguinity.

Geochronologic, geochemical, and petrographic data indicate that the Stevens, Reflection-Pyramid, and Nisqually plutons each represent a discrete pulse of crystal-rich magma. Each of the Tatoosh intrusive suite plutons is distinguished by a relatively evolved diagnostic composition that became variably modified toward crystal cumulates by interstitial melt extraction. Enclaves, plagioclase characteristics, and geochemical systematics suggest that magma mixing, involving multiple components, may also have contributed to Tatoosh intrusive suite petrogenesis. Geochemically distinct zircon crystals in each of the Tatoosh intrusive suite plutons and the absence of Stevens-age zircon antecrysts in the Reflection-Pyramid pluton indicate that the Reflection-Pyramid pluton cannot represent a mixing product involving the Stevens and Nisqually magmas. The Pyramid phase is a marginal cumulate coeval and cogenetic with the Reflection phase.

Trace-element concentrations in Tatoosh intrusive suite zircons have large ranges in single rock samples that imply relatively late zircon crystallization in isolated pockets of variably evolved but highly differentiated residual liquid. Values of Eu/Eu* in relation to Hf concentration in zircon show discrete trends for Nisqually versus Reflection-Pyramid samples, whereas Stevens zircons display two trends, one similar to Reflection-Pyramid and another with much higher Eu/Eu* than for zircon from the other plutons. Zircon crystals typically are zoned to higher Hf concentrations and to lower Th/U ratios and U and Th concentrations. Late overgrowths and reentrant infillings have high U and Hf, low Th, Th/U, and Eu/Eu* that suggest crystallization near the magma-hydrothermal transition. Chondrite-normalized REE patterns for zircon have familiar steeply positive slopes, convex-upward shapes, positive Ce anomalies, and negative Eu anomalies. As with other trace elements, REE concentrations in Tatoosh intrusive suite zircon have one to two orders of magnitude ranges in single samples and show consistent zoning trends between crystal interiors and margins. Collectively, the zircon trace-element data help to group geochemically related samples and constrain zircon crystallization environments.

The Tatoosh intrusive suite preserves manifestations of shallow hydrothermal systems similar to those presently active within some modern High Cascades magmatic systems, including Mount Rainier (John et al., 2008). However, hydrothermal systems associated with the Tatoosh intrusive suite were generally weak and not known to have developed porphyry copper systems such as those related to several other Miocene plutons in the ancestral Cascades arc in Washington (Hollister, 1979; John et al., 2003; Blakely et al., 2007). Tatoosh intrusive suite rocks were variably affected by hydrothermal activity that accompanied emplacement and solidification of Tatoosh intrusive suite magmas; fluid inclusion characteristics, weak deuteric alteration, and widely spaced metal-poor veins indicate the former ubiquitous presence of magmatically derived hydrothermal fluids.

The absence of argillic-, advanced argillic-, and phyllic- (sericitic) altered rocks, which precludes interaction with circulating acidic fluids, probably reflects relatively low magmatic sulfur contents, low HCl and HF contents, and (or) relatively reducing conditions that resulted in low SO_2/H_2S ratios. Early crystallization of magmatic sulfides in the Stevens pluton and Pyramid phase and the apparent absence of magmatic anhydrite in all Tatoosh intrusive suite units suggest a low to moderate magmatic oxidation state, as does the absence of magnetite in the Pyramid phase. Copper contents of the Nisqually and Reflection-Pyramid plutons remained relatively high throughout crystallization, suggesting that Cu remained in the crystallizing magmas and was not concentrated in magmatic-hydrothermal fluids. Halite-saturated and vapor-rich fluid inclusions are present in most parts of the Tatoosh intrusive suite, but these inclusions lack chalcopyrite daughter crystals characteristic of hydrothermal fluids related to porphyry copper systems (Bodnar, 1995), also indicating that Cu remained in the crystallizing magmas. Low sulfide (including pyrite) contents in altered rocks and veins suggest that hydrothermal fluids associated with the Tatoosh intrusive suite had low sulfur contents. These observations suggest relatively reduced, sulfur-poor(?) magmas that partially degassed during ascent and experienced bursts of H_2O-rich vapor exsolution relatively late during their crystallization, as suggested by early pyroxene crystallization and late hornblende crystallization; therefore, they did not develop strong hydrothermal systems capable of porphyry copper deposit formation.

Geochemical characteristics that distinguish the Stevens, Nisqually, and Reflection-Pyramid plutons were likely inherited from their respective sources. Textural, mineralogic, and geochemical features preserved in these shallowly emplaced plutons illustrate processes that must also prevail during solidification of more deeply emplaced plutonic to batholithic bodies that are typically coarser grained. These characteristics, and the apparent lack of significant internal contacts or internal discontinuities, suggest that each magma body was largely homogenized and experienced differential interstitial liquid loss somewhat before shallow intrusion in a fashion inconsistent with coupled incremental-emplacement solidification histories.

ACKNOWLEDGMENTS

We thank the National Park Service for permission to work within Mount Rainier National Park and collect samples. Reviews by T.W. Sisson and K.A. Howard improved an early version of this manuscript, and *GSA Bulletin* reviewers J.M. Mattinson and G.A.R. Gualda, as well as Associate Editor C.F. Miller, substantially sharpened the presentation of our study. This work was funded by the U.S. Geological Survey Mineral Resources Program. V.J.M. Salters generously provided radiogenic isotope data through support from National Science Foundation (NSF) grants OCE-0648484 and EAR-0635864.

REFERENCES CITED

Anders, E., and Ebihara, M., 1982, Solar-system abundances of the elements: Geochimica et Cosmochimica Acta, v. 46, p. 2363–2380, doi: 10.1016/0016-7037(82)90208-3.

Anders, E., and Grevesse, N., 1989, Abundances of the elements—Meteoritic and solar: Geochimica et Cosmochimica Acta, v. 53, p. 197–214, doi: 10.1016/0016-7037(89)90286-X.

Andrews, B.J., Gardner, J.E., and Housh, T.B., 2008, Repeated recharge, assimilation, and hybridization in magmas erupted from El Chichon as recorded by plagioclase and amphibole phenocrysts: Journal of Volcanology and Geothermal Research, v. 175, p. 415–426, doi: 10.1016/j.jvolgeores.2008.02.017.

Bachl, C.A., Miller, C.F., Miller, J.S., and Faulds, J.E., 2001, Construction of a pluton: Evidence from an exposed cross section of the Searchlight pluton, Eldorado Mountains, Nevada: Geological Society of America Bulletin, v. 113, p. 1213–1228, doi: 10.1130/0016-7606(2001)113<1213:COAPEF>2.0.CO;2.

Bachmann, O., and Bergantz, G.W., 2004, On the origin of crystal-poor rhyolites; extracted from batholithic crystal mush: Journal of Petrology, v. 45, p. 1565–1582, doi: 10.1093/petrology/egh019.

Bacon, C.R., and Lowenstern, J.B., 2005, Late Pleistocene granodiorite source for recycled zircon and phenocrysts in rhyodacite lava at Crater Lake, Oregon: Earth and Planetary Science Letters, v. 233, p. 277–293, doi: 10.1016/j.epsl.2005.02.012.

Bateman, P.C., 1992, Plutonism in the Central Part of the Sierra Nevada Batholith, California: U.S. Geological Survey Professional Paper 1483, 186 p.

Belousova, E.A., Griffin, W.L., O'Reilly, S.Y., and Fisher, N.I., 2002, Igneous zircon—Trace element composition as an indicator of source rock type: Contributions to Mineralogy and Petrology, v. 143, p. 602–622.

Blakely, R.J., John, D.A., Box, S.E., Berger, B.R., Fleck, R.J., Ashley, R.P., Newport, G.R., and Heinemeyer, G.R., 2007, Crustal controls on magmatic-hydrothermal systems—A geophysical comparison of White River, Washington, with Goldfield, Nevada: Geosphere, v. 3, p. 91–107, doi: 10.1130/GES00071.1.

Blundy, J., and Wood, B., 2003, Mineral-melt partitioning of uranium and thorium and their daughters, *in* Bourdon, B., Henderson, G.M., Lundstrom, C.C., and Turner, S.P., eds., Uranium-Series Geochemistry: Reviews in Mineralogy and Geochemistry, v. 52, p. 59–123.

Bodnar, R.J., 1995, Fluid inclusion evidence for magmatic source for metals in porphyry copper deposits, *in* Thompson, J.F.H., ed., Magmas, Fluids, and Ore Deposits: Mineralogical Association of Canada Short Course Handbook, v. 25, p. 139–152.

Brown, S.J.A., and Fletcher, I.R., 1999, SHRIMP U-Pb dating of the preeruption growth history of zircons from the 340 ka Whakamaru Ignimbrite, New Zealand—Evidence for >250 k.y. magma residence times: Geology, v. 27, p. 1035–1038, doi: 10.1130/0091-7613(1999)027<1035:SUPDOT>2.3.CO;2.

Cameron, K.L., and Cameron, M., 1985, Rare earth element, $^{87}Sr/^{86}Sr$, and $^{143}Nd/^{144}Nd$ compositions of Cenozoic orogenic dacites from Baja California, northwestern Mexico, and adjacent West Texas; evidence for the predominance of a subcrustal component: Contributions to Mineralogy and Petrology, v. 91, p. 1–11, doi: 10.1007/BF00429422.

Charlier, B.L.A., Wilson, C.J.N., Lowenstern, J.B., Blake, S., van Calsteren, P.W., and Davidson, J.P., 2005, Magma generation at a large, hyperactive silicic volcano (Taupo, New Zealand) revealed by U-Th and U-Pb systematics in zircons: Journal of Petrology, v. 46, p. 3–32, doi: 10.1093/petrology/egh060.

Claiborne, L.L., Miller, C.F., Walker, B.A., Wooden, J.L., Mazdab, F.K., and Bea, F., 2006, Tracking magmatic processes through Zr/Hf ratios in rocks and Hf and Ti zoning in zircons—An example from the Spirit Mountain batholith, Nevada: Mineralogical Magazine, v. 70, p. 517–543, doi: 10.1180/0026461067050348.

Coleman, D.S., Gray, W., and Glazner, A.F., 2004, Rethinking the emplacement and evolution of zoned plutons; geochronologic evidence for incremental assembly of the Tuolumne intrusive suite, California: Geology, v. 32, p. 433–436.

Crowley, J.L., Schoene, B., and Bowring, S.A., 2007, U-Pb dating of zircon in the Bishop Tuff at the millennial scale: Geology, v. 35, p. 1123–1126, doi: 10.1130/G24017A.1.

Davidson, J.P., Morgan, D.J., Charlier, B.L.A., Harlou, R., and Hora, J.M., 2007, Microsampling and isotopic analysis of igneous rocks: Implications for the study of magmatic systems: Annual Review of Earth and Planetary Sciences, v. 35, p. 273–311, doi: 10.1146/annurev.earth.35.031306.140211.

du Bray, E.A., John, D.A., Sherrod, D.R., Evarts, R.C., Conrey, R.M., and Lexa, Jaroslav, 2006, Geochemical Database for Volcanic Rocks of the Western Cascades, Washington, Oregon, and California: U.S. Geological Survey Data Series Report DS-0155, 49 p.

Ewart, A., 1982, The mineralogy and petrology of Tertiary-Recent orogenic volcanic rocks with special reference to the andesitic-basaltic compositional range, *in* Thorpe, R.S., ed., Andesites: Chichester, UK, Wiley, p. 25–87.

Feeley, T.C., and Davidson, J.P., 1994, Petrology of calc-alkaline lavas at Volcan Ollaguee and the origin of compositional diversity at central Andean stratovolcanoes: Journal of Petrology, v. 35, p. 1295–1340.

Fiske, R.S., Hopson, C.A., and Waters, A.C., 1963, Geology of Mount Rainier National Park, Washington: U.S. Geological Survey Professional Paper 444, 93 p.

Frost, B.R., Barnes, C.G., Collins, W.J., Arculus, R.J., Ellis, D.J., and Frost, C.D., 2001, A geochemical classification for granitic rocks: Journal of Petrology, v. 42, p. 2033–2048, doi: 10.1093/petrology/42.11.2033.

GEOROC, 2007, Geochemistry of Rocks of the Oceans and Continents: Max-Plank-Institut für Chemie: http://georoc.mpch-mainz.gwdg.de/georoc/ (accessed July 2009).

Gill, J., 1981, Orogenic Andesites and Plate Tectonics: New York, Springer-Verlag, 390 p.

Glazner, A.F., Bartley, J.M., Coleman, D.S., Gray, W., and Taylor, R.Z., 2004, Are plutons assembled over millions of years by amalgamation from small magma chambers?: GSA Today, v. 14, no. 4–5, p. 4–11.

Hanson, G.N., 1980, Rare earth elements in petrogenetic studies of igneous systems: Annual Review of Earth and Planetary Sciences, v. 8, p. 371–406, doi: 10.1146/annurev.ea.08.050180.002103.

Harper, B.E., Miller, C.F., Koteas, G.C., Cates, N.L., Wiebe, R.A., Lazzareschi, D.S., and Cribb, J.W., 2004, Granites, dynamic magma chamber processes and pluton construction: The Aztec Wash pluton, Eldorado Mountains, Nevada, USA: Transactions of the Royal Society of Edinburgh–Earth Sciences, v. 95, p. 277–295, doi: 10.1017/S0263593300001073.

Hildreth, W., and Wilson, C.J.N., 2007, Compositional zoning of the Bishop Tuff: Journal of Petrology, v. 48, p. 951–999, doi: 10.1093/petrology/egm007.

Hirt, W.H., 2007, Petrology of the Mount Whitney intrusive suite, eastern Sierra Nevada, California; implications for the emplacement and differentiation of composite felsic intrusions: Geological Society of America Bulletin, v. 119, p. 1185–1200, doi: 10.1130/B26054.1.

Hollister, V.F., 1979, Porphyry copper deposits of the Cascade volcanic arc, Washington: Minerals Science and Engineering, v. 11, p. 22–34.

Hoskin, P.W.O., and Schaltegger, U., 2003, The composition of zircon and igneous and metamorphic petrogenesis, *in* Hanchar, J.M., and Hoskin, P.W.O., eds., Zircon: Reviews in Mineralogy and Geochemistry, v. 53, p. 27–62.

Ireland, T.R., and Williams, I.S., 2003, Considerations in zircon geochronology by SIMS, *in* Hanchar, J.M., and Hoskin, P.W.O., eds., Zircon: Reviews in Mineralogy and Geochemistry, v. 53, p. 215–241.

Irvine, T.N., and Baragar, W.R.A., 1971, A guide to the chemical classification of the common volcanic rocks: Canadian Journal of Earth Sciences, v. 8, p. 523–548.

John, D.A., Rytuba, J.J., Ashley, R.P., Blakely, R.J., Vallance, J.W., Newport, G.R., and Heinemeyer, G.R., 2003, Field Guide to Hydrothermal Alteration in the White River Altered Area and in the Osceola Mudflow, Washington: U.S. Geological Survey Bulletin 2217, 58 p.

John, D.A., Sisson, T.W., Breit, G.N., Rye, R.O., and Vallance, J.W., 2008, Characteristics, extent and origin of hydrothermal alteration at Mount Rainier volcano, Cascades Arc, USA—Implications for debris-flow hazards and mineral deposits: Journal of Volcanology and Geothermal Research, v. 175, p. 289–314, doi: 10.1016/j.jvolgeores.2008.04.004.

Korotev, R.L., 1996, A self-consistent compilation of elemental concentration data for 93 geochemical reference samples: Geostandards Newsletter, v. 20, p. 217–245, doi: 10.1111/j.1751-908X.1996.tb00185.x.

Le Maitre, R.W., 1989, A Classification of Igneous Rocks and Glossary of Terms: Oxford, UK, Blackwell Scientific, 193 p.

Lipman, P.W., 2007, Incremental assembly and prolonged consolidation of Cordilleran magma chambers; evidence from the Southern Rocky Mountain volcanic field: Geosphere, v. 3, p. 42–70, doi: 10.1130/GES00061.1.

Ludwig, K.A., 2003, Isoplot/Ex Ver. 3.00, A Geochronological Tool Kit for Microsoft Excel: Berkeley Geochronology Center Special Publication 4, 70 p.

Ludwig, K.A., and Mundil, R., 2002, Extracting reliable U-Pb ages and errors from complex populations of zircons from Phanerozoic tuffs: Geochimica et Cosmochimica Acta, v. 66, no. 15A, p. 463.

Mattinson, J.M., 1977, Emplacement history of the Tatoosh volcanic-plutonic complex, Washington: Ages of zircons: Geological Society of America Bulletin, v. 88, p. 1509–1514, doi: 10.1130/0016-7606(1977)88<1509:EHOTTV>2.0.CO;2.

Matzel, J.E.P., Bowering, S.A., and Miller, R.B., 2006, Time scales of pluton construction at differing crustal levels—Examples from the Mount Stuart and Tenpeak intrusions, North Cascades, Washington: Geological Society of America Bulletin, v. 118, p. 1412–1430, doi: 10.1130/B25923.1.

McBirney, A.R., 1978, Volcanic evolution of the Cascade Range: Earth and Planetary Science Annual Reviews, v. 6, p. 437–456, doi: 10.1146/annurev.ea.06.050178.002253.

Miller, C.F., and Wark, D.A., 2008, Supervolcanoes and their explosive supereruptions: Elements, v. 4, p. 11–16, doi: 10.2113/GSELEMENTS.4.1.11.

Miller, J.S., Matzel, J.E.P., Miller, C.F., Burgess, S.D., and Miller, R.B., 2007, Zircon growth and recycling during the assembly of large, composite arc plutons: Journal of Volcanology and Geothermal Research, v. 167, p. 282–299, doi: 10.1016/j.jvolgeores.2007.04.019.

Miyashiro, A., 1974, Volcanic rock series in island arcs and active continental margins: American Journal of Science, v. 274, p. 321–355.

Moore, J.G., and Sisson, T.W., 2008, Igneous phenocrystic origin of K-feldspar megacrysts in granitic rocks from the Sierra Nevada batholith: Geosphere, v. 4, p. 387–400, doi: 10.1130/GES00146.1.

Pearce, J.A., Harris, N.B.W., and Tindle, A.G., 1984, Trace element discrimination diagrams for the tectonic interpretation of granitic rocks: Journal of Petrology, v. 25, p. 956–983.

Priest, G.R., 1990, Volcanic and tectonic evolution of the Cascade volcanic arc, central Oregon: Journal of Geophysical Research, v. 95, no. B12, p. 19,583–19,599, doi: 10.1029/JB095iB12p19583.

Reid, M.R., 2003, Timescales of magma transfer and storage in the crust, *in* Holland, H.D., and Turekian, K.K., eds., Treatise on Geochemistry, Volume 3: Amsterdam, Elsevier, p. 167–193.

Sambridge, M.S., and Compston, W., 1994, Mixture modeling of multi-component data sets with application to ion-probe zircon ages: Earth and Planetary Science Letters, v. 128, p. 373–390, doi: 10.1016/0012-821X(94)90157-0.

Shand, S.J., 1951, Eruptive Rocks: New York, John Wiley, 488 p.

Simon, A.C., Pettke, T., Candela, P.A., Piccoli, P.M., and Heinrich, C.A., 2006, Copper partitioning in a melt-vapor-brine-magnetite-pyrrhotite assemblage: Geochimica et Cosmochimica Acta, v. 70, p. 5583–5600, doi: 10.1016/j.gca.2006.08.045.

Sisson, T.W., 2005, Solidification, zoning, and homogenization in Sierran plutons: Geological Society of America Abstracts with Programs, v. 37, no. 4, p. 39.

Sisson, T.W., and Bacon, C.R., 1999, Gas-driven filter pressing in magmas: Geology, v. 27, p. 613–616, doi: 10.1130/0091-7613(1999)027<0613:GDFPIM>2.3.CO;2.

Smith, J.G., 1993, Geologic Map of Upper Eocene to Holocene Volcanic and Related Rocks in the Cascade Range, Washington: U.S. Geological Survey Miscellaneous Investigations Series Map I-2005, scale 1:500,000, 19 p.

Streckeisen, A., 1976, To each plutonic rock its proper name: Earth-Science Reviews, v. 12, p. 1–33, doi: 10.1016/0012-8252(76)90052-0.

Thompson, M.E., 1983, Solidification in Magmas: Part 1. The Magmatic History of the Tatoosh Volcanic-Plutonic Complex, Mount Rainier National Park; Part 2. Numerical Simulation of Heat and Mass Transfer in Solidifying Magmas [M.S. thesis]: Eugene, University of Oregon, 227 p.

Vance, J.A., Clayton, G.A., Mattinson, J.M., and Naeser, C.W., 1987, Early and Middle Cenozoic stratigraphy of the Mount Rainier–Tieton River area, southern Washington Cascades, *in* Schuster, J.E., ed., Selected Papers on the Geology of Washington: Washington Division of Geology and Earth Resources Bulletin 77, p. 269–290.

Vernon, R.H., 1984, Microgranitoid enclaves in granites; globules of hybrid magma quenched in a plutonic environment: Nature, v. 309, p. 438–439, doi: 10.1038/309438a0.

Walker, B.A., Miller, C.F., Claiborne, L.L., Wooden, J.L., and Miller, J.S., 2007, Geology and geochronology of the Spirit Mountain batholith, southern Nevada: Implications for timescales and physical processes of batholith construction: Journal of Volcanology and Geothermal Research, v. 167, no. 1–4, p. 239–262, doi: 10.1016/j.jvolgeores.2006.12.008.

Wark, D.A., 1991, Oligocene ash flow volcanism, northern Sierra Madre Occidental; role of mafic and intermediate-composition magmas in rhyolite genesis: Journal of Geophysical Research, v. 96, p. 13,389–13,411, doi: 10.1029/90JB02666.

Watson, E.B., 1979, Zircon saturation in felsic liquids; experimental results and applications to trace element geochemistry: Contributions to Mineralogy and Petrology, v. 70, p. 407–419, doi: 10.1007/BF00371047.

Watson, E.B., 1996, Dissolution, growth and survival of zircons during crustal fusion; kinetic principles, geological models and implications for isotopic inheritance: Transactions of the Royal Society of Edinburgh–Earth Sciences, v. 87, p. 43–56.

White, C.M., and McBirney, A.R., 1978, Some quantitative aspects of orogenic volcanism in the Oregon Cascades, *in* Smith, R.B., and Eaton, G.P., eds., Cenozoic Tectonics and Regional Geophysics of the Western Cordillera: Geological Society of America Memoir 152, p. 369–388.

Wood, D.A., Joron, J.L., and Treuil, M., 1979, A re-appraisal of the use of trace elements to classify and discriminate between magma series erupted in different tectonic settings: Earth and Planetary Science Letters, v. 45, p. 326–336, doi: 10.1016/0012-821X(79)90133-X.

Wright, T.L., 1961, The Mineralogy and Petrogenesis of the Southern Part of the Tatoosh Pluton, Mount Rainier National Park, Washington [Ph.D. dissertation]: Baltimore, Maryland, Johns Hopkins University, 324 p.

Zak, J., and Paterson, S.R., 2005, Characteristics of internal contacts in the Tuolumne batholith, central Sierra Nevada, California (USA); implications for episodic emplacement and physical processes in a continental arc magma chamber: Geological Society of America Bulletin, v. 117, p. 1242–1255, doi: 10.1130/B25558.1.

Manuscript Received 26 May 2009
Revised Manuscript Received 23 March 2010
Manuscript Accepted 29 March 2010

Printed in the USA